IDENTIFICATION OF A FUNCTIONALLY ESSENTIAL AMINO ACID FOR AN *ARABIDOPSIS* CYCLIC NUCLEOTIDE-GATED ION CHANNEL

by

Joyce Baxter

A thesis submitted in conformity with the requirements

for the degree of Master of Science

Graduate Department of Cell and Systems Biology

University of Toronto

Your file Votre référence
ISBN: 978-0-494-40100-2
Our file Notre référence
ISBN: 978-0-494-40100-2

IDENTIFICATION OF A FUNCTIONALLY ESSENTIAL AMINO ACID FOR THE *ARABIDOPSIS* CYCLIC NUCLEOTIDE-GATED ION CHANNEL ATCNGC11/12

Joyce Baxter
Masters of Science 2007
Graduate Department of Cell and Systems Biology
University of Toronto

ABSTRACT

The *cpr22 Arabidopsis* mutant shows constitutive activation of pathogen resistance responses and has spontaneous lesions. *cpr22* was identified to encode for a novel chimeric gene, *ATCNGC11/12*, created by a fusion between *ATCNGC11* and *12*. Previous analyses suggested that ATCNGC11/12 forms a functional cAMP-activated CNGC in yeast and that the phenotype conferred by *cpr22* is attributable to the expression of *ATCNGC11/12*. To identify downstream components of the *cpr22*-mediated signal transduction pathway or identify functionally important residues of this channel, a genetic screen for mutants that suppress *cpr22*-related phenotypes was conducted. One suppressor, #73 was identified to have an intragenic mutation in *ATCNGC11/12*. In this project, I have characterized the #73 mutant and analyzed the mechanism to suppress the *cpr22* phenotypes by this mutation. This mutation, E519K, is located in the cyclic nucleotide binding domain. Our computational modeling suggests that this mutation alters an important amino acid necessary for channel activity and intra/inter subunit interactions that stabilize the tertiary channel structure.

LIST OF ABBREVIATIONS

A. tumefaciens	*Agrobacterium tumefaciens*
bp	base pair
°C	degrees Centigrade
cDNA	complementary DNA
cAMP	cyclic adenosine monophosphate
cGMP	cyclic guanosine monophospate
CNGC	cyclic nucleotide gated ion channel
CNBD	cyclic nucleotide binding domain
Col-0	Columbia-0
dATP	deoxyadenosine triphosphate
dCTP	deoxycytidine triphophate
ddH_2O	double distilled water
dGTP	deoxyguanosine triphosphate
DNA	deoxyribonucleic acid
dNTP	deoxynucleotide triphosphate
dpi	days post inoculation
DTT	1,4-dithiothreitol
dTTP	deoxythymidine triphosphate
E. coli	*Escherichia coli*
EDTA	ethylenediaminetetra-acetic acid
EMS	ethylmethane sulphonate
EtBr	ethidium bromide
EtOH	ethanol
g	gram
GFP	green fluorescent protein
His	histidine
H. parasitica	*Hyaloperonospora parasitica*
hr	hour(s)
HR	hypersensitive response
IPTG	isopropyl-β-D-thiogalactopyranoside
JA	jasmonic acid
KDa	kilodalton
KO12	knock-out of the *ATCNGC12* gene in *Arabidopsis*
L	litre
LB	Luria-Bertani broth
LiAc	lithium acetate
m	metre
M	molar
MES	2-(4-Morpholino)ethanesulfonic acid
min	minute(s)
mol	mole(s)
MS	Murashige and Skoog media
NaCL	sodium chloride
NCBI	National Center forBiotechnology Information
N. benthamaina	*Nicotiana benthamiana*

OD	optical density
PAGE	polyacrylamide gel electrophoresis
PCR	polymerase chain reaction
PEG	polyethylene glycol
PHYRE	protein homology/analogy recognition engine
PR	pathogenesis-related
psi	pounds per square inch
PVDF	Polyvinylidene fluoride
RNA	ribonucleic acid
rpm	revolutions per minute
RH	relative humidity
RT	room temperature
RT-PCR	reverse transcriptase polymerase chain reaction
SA	salicylic acid
SC	synthetic complete
sec	second(s)
SDS	sodium dodecylsulfate
smGFP	soluble modified green fluorescence protein
TAE	tris-acetate-EDTA electrophoresis buffer
TE	tris EDTA
T_m	melting temperature
Tris	N, N, N', N'-tetramethylethylethylenediamine
μ	micro
ura	uracil
V	volts
vol	volume
v/v	volume per volume
w	weight
Ws	Wassilewskija
wt	wildtype
X-gal	5-bromo-4-chloro-3-indolyl-β-D-galactopyranoside
YPD	yeast extract/peptone/dextrose

TABLE OF CONTENTS

Statement of Publication

The research presented in this thesis has been presented in the Annual Meeting of the Canadian Society of Plant Physiologists (CSPP) (McMaster University, Hamilton, 2006) and in the Annual Meeting of the American Society of Plant Biologist (Chicago, 2007) and is currently in preparation for original publication in the Plant Journal.

LIST OF FIGURES

LIST OF TABLES

CHAPTER 1 - Introduction

In this thesis, I have studied a functionally essential amino acid for the *Arabidopsis* cyclic nucleotide-gated ion channel (CNGC), *ATCNGC11/12*. To provide the background of this research, I have summarized the literature reviews of CNGCs and the previous findings in the Yoshioka laboratory, at the University of Toronto.

1.1 Animal CNGCs

1.1.1 Discovery of animal CNGCs and their biological role

Cyclic nucleotide-gated ion channels (CNGCs) are nonselective cation channels. They were first discovered in vertebrate rod photoreceptors at the plasma membrane where they play a critical role in phototransduction (Fesenko *et al.*, 1985). Following this discovery, CNGCs were also found to play a role for odorant signal transduction in olfactory neurons (Nakamura & Gold, 1987). CNGCs have also been found in nonsensory tissues such as the hippocampus, heart, testis, kidney, pancreas, adrenal gland and colon (Kaupp and Seifert, 2002). However, the role of these channels in nonsensory tissues is not as well known as for the rod and olfactory CNGCs.

The activation of rod photoreceptors occurs in the dark when cGMP molecules bind to a channel. Full activation will lead to an open channel, whereby an inward current of ions flows into the cell. When light hits the retina a phototransduction cascade occurs, causing the hyrolysis of cGMP to GMP. As a response to the decrease in cGMP in the cell, the CNGCs will close. Closing of the CNGCs reduces the cytoplasmic Ca^{2+} concentration which then acts as a negative feedback in the phototransduction cascade by

stimulating cGMP synthesis while simultaneously increasing the channel's affinity for cGMP (Matulef and Zagotta, 2003).

Along with rod photoreceptors, CNGCs have also been identified in cone photoreceptors and are activated by the same fundamental events of phototransduction in rods (Kaupp and Seifert, 2002). Cone photoreceptors are sensitive to a wider range of light intensities than rods and it remains that cGMP is also their ligand necessary for activation. Whereas, the transduction of odorant signals through olfactory CNGCs are activated by cAMP (Nakamura and Gold, 1987).

So far, six members of the CNGC gene family have been identified in vertebrates. Based on sequence similarity, these genes were classified into two subtypes, CNGA (CNGA1-4) and CNGB (CNGB1 and 3) (Bradley *et al.*, 2001a). The first cDNA clone for a subunit of a rod channel, CNGA1, was isolated from bovine retina (Kaupp *et al.*, 1989) and the second subunit of a bovine rod channel, CNGB1, was later isolated and cloned (Körschen *et al.*, 1995).

Mutations in rod or cone, and olfactory channel subunits can cause different forms of blindness or a loss of odorant signaling, respectively. In the CNGA1 of rod channels, a mutation can cause an autosomal recessive form of retinitis pigmentosa (a degenerative form of blindness) in humans (Dryja *et al.*, 1995). Whereas, mutations in CNGA3 and CNGB3 of channels in cone photoreceptors have been connected to causing complete achromatopsia (total colour blindness) (Kohl *et al.*, 1998, 2000; Sundin *et al.*, 2000; Wissinger *et al.*, 2001). In olfactory neurons, mice lacking CNGA2 have total anosmia (lost the ability to smell) (Brunet *et al.*, 1996). However, when the mice lacked

CNGA4 they exhibited abnormal olfactory capabilities (Bradley *et al.*, 2001b; Munger *et al.*, 2001).

1.1.2 Structure of animal CNGCs

The structure of an animal CNGC subunit is comprised of six transmembrane domains (S1-S6), a P-loop, an intracellular amino-terminal and carboxy-terminal regions (Figure 1) (Matulef and Zagotta, 2003). The structure of each subunit is similar to that of the voltage-gated, outward rectifying K^+-selective ion channel (Shaker) proteins. The P-loop located between S5 and S6 transmembrane domain creates the ion-conducting pore. The S4 domain contains a charged sequence motif that resembles the voltage-sensor motif found in the S4 domain of Shaker-type voltage sensor channels (Kaupp and Seifert, 2002). This suggest that that CNGCs may be able to gate by voltage sensing, however experimental the study showed that they are predominantly gated by ligand binding. The cytoplasmic carboxy-terminal region contains a cyclic nucleotide-binding domain (CNBD) with a segment that connects the S6 segment and the CNBD, known as the C-linker. A calmodulin binding domain (CaMBD) resides in the cytosolic amino terminus of a subunit (Figure 1).

It has been suggested that animal CNGCs form heterotetramers with their subunits varying depending on the tissue types where they are present (Gordon and Zagotta, 1995; Liu *et al.*, 1996; Varnum and Zagotta, 1996). Native rod channels are thought to be composed of three CNGA1 subunits and one CNGB1 subunit (Weitz *et al.*, 2002; Zheng *et al.*, 2002; Zhong *et al.*, 2002). Although, when expressed heterologously, CNGA subunits form functional homomeric channels but not CNGB subunits (Zagotta

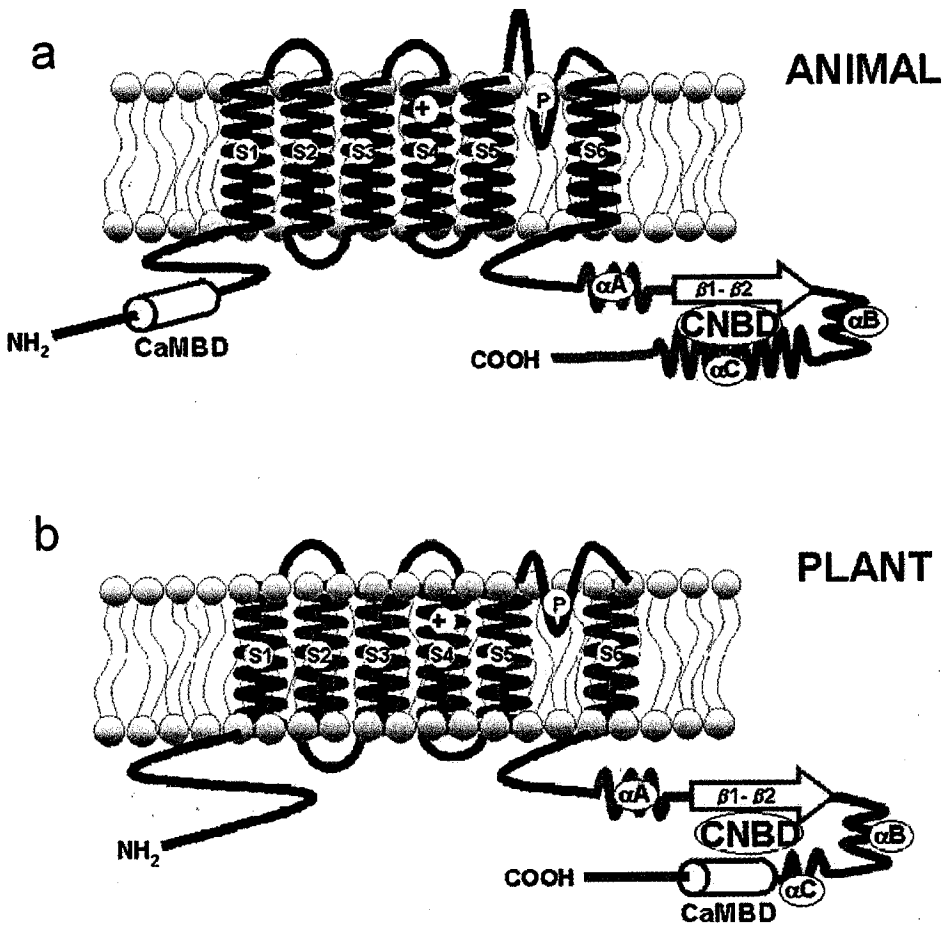

Figure 1. Comparison of animal (a) and plant (b) predicted CNGC membrane topology. Transmembrane domains (S1-S6), with a pore region (P) are identified. The CNBD for both animal and plant CNGCs are located at the cytosolic C-terminus which incorporate three α-helices (A-C) and two β-sheets (made up of eight β-strands). The major structural difference between animal and plant CNGCs is the location of the CaMBD in the N-terminus or the C-terminus, respectively. (Taken from Hua *et al.*, 2003).

and Siegelbaum, 1996; Kaupp and Zagotta, 2002). Native olfactory channels are thought to be composed of three different subunits, CNGA2 or CNGA4, and a form of CNGB1 (Matulef and Zagotta, 2003).

1.2 Plant CNGCs

1.2.1 Discovery of plant CNGCs and its biological role

The first plant CNGC was identified as a CaM binding protein from the plasma membrane of barley aleurone (HvCBT1) (Schuurink *et al.*, 1998). HvCBT1 was identified by screening a cDNA expression library from barley aleurone with an *Arabidopsis* calmodulin protein (AtCaM2) (Schuurink *et al.*, 1998). Subsequently, several CNGCs were identified from *Arabidopsis* and *Nicotiana tabacum* (Köhler and Neuhaus, 1998; Arazi *et al.*, 1999; Leng *et al.*, 1999; Köhler and Neuhaus, 1999; Li *et al.*, 2005; Gobert *et al.*, 2006). The completion of the *Arabidopsis* genome sequencing project revealed a large family of CNGC genes, consisting of twenty members (Mäser *et al.*, 2001). Bioinformatic tools were used to categorize *Arabidopsis* CNGCs by protein sequence similarity which then divided them into five different subgroups (I-IVB) (Figure 2; Mäser *et al.*, 2001). Considering that only six CNGC genes were found in animal genomes, the large size of this gene family in plants suggests a diversity and importance in physiological functions. Due to the size of the gene family, a complete understanding of the biological role of plant CNGCs may take some time. One method to assist in predicting the possible partner/physiological role of ATCNGCs, is the expression pattern of these genes. A tissue-specific expression analysis for all 20 ATCNGCs has been reported using expressed sequence tag (EST) data (Talk *et al.*,

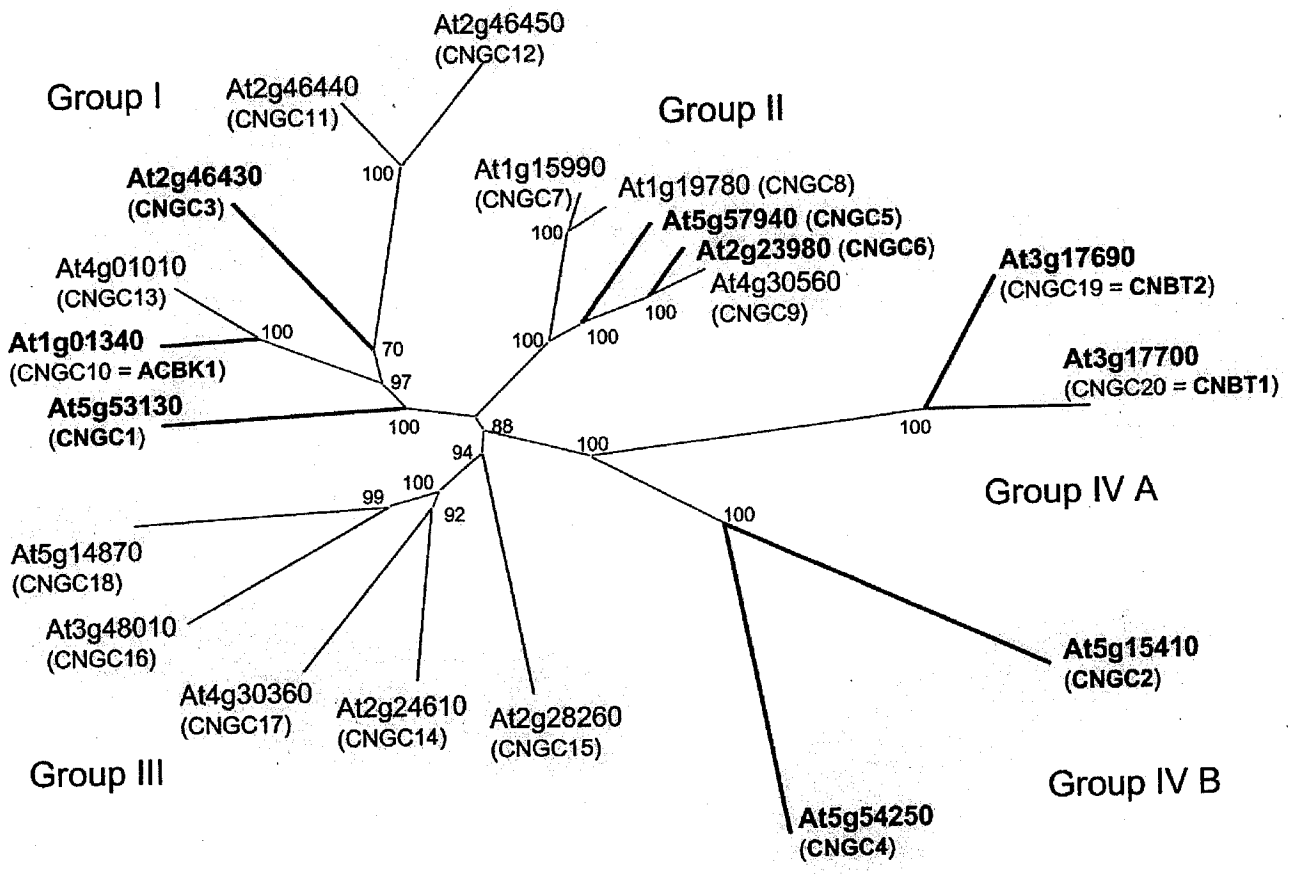

Figure 2. Phylogenetic tree using protein sequences of the 20-membered CNGC family in *Arabidopsis*. The 20 members are organized into five groups (I-IVB) based on sequence similarity. (Taken from Mäser *et al.*,2001).

2003). In this analysis, it was found that the *Arabidopsis* CNGCs are expressed differentially in all tissues.

So far, possible biological functions of group I and group IVB members have been reported (Köhler *et al.*, 2001; Sunkar *et al.*, 2000; Balague *et al.*, 2003; Chan *et al.*, 2003; Li *et al.*, 2005; Ma *et al.*, 2006; Gobert *et al.*, 2006; Yoshioka *et al.*, 2006; Borsics *et al.*, 2007). ATCNGC10 appears to be important throughout plant development, particularly in root growth, while ATCNGC1 has been shown to participate in heavy metal movement (Sunkar *et al.*, 2000; Ma *et al.*, 2006; Borsics *et al.*, 2007; Christopher *et al.*, 2007). ATCNGC3 has been shown to be involved in the uptake and/or translocation of K^+ and Na^+ and therefore, may be necessary to maintain homeostasis of these ions (Gobert *et al.*, 2006). ATCNGC2 and 4 have been suggested to play a role in pathogen response (Clough *et al.*, 2000; Balague *et al.*, 2003).

ATCNGC2 and *4* are members of the most divergent groups, IVB. Null mutations for *ATCNGC2* and *4* were found in the *Arabidopsis* mutant *dnd1* (Yu *et al.*, 1998; Clough *et al.*, 2000) and *dnd2/hlm1* (Balague *et al.*, 2003; Jurkowski *et al.*, 2004), respectively. Both *dnd1* and *dnd2/hlm1* share striking similarity in pathogen resistance phenotypes. These phenotypes include the accumulation of salicylic acid (SA), constitutive expression of pathogenesis related (*PR*) genes and an altered hypersensitive response (HR), which would induce localized cell death at the site of invasion. SA is thought to be a common signaling molecule during pathogen resistance responses to activate defense genes, such as *PR* genes or initiate the HR (Dangl *et al.*, 1996; Hammond-Kosack and Jones, 1996; Dempsey *et al.*, 1999). Additionally, the barley homolog of *ATCNGC4* has been identified as *NEC1*. The *nec1* mutant shows necrotic spots on green tissues visually

resembling HR (Rostoks *et al.*, 2006). Along with a role in pathogen resistance, *ATCNGC2* seems to be involved in development and innate immunity (Köhler *et al.*, 2001; Chan *et al.*, 2003; Ali *et al.*, 2006).

1.2.2 Structure of Plant CNGCs

As shown in Figure 1, the predicted structure of a plant CNGC subunit is almost identical to that of animal CNGCs. It consists of six transmembrane domains, one pore region and a CNBD at the carboxy terminal. The only difference is the location of the CaMBD. The location of the CaMBD in animal CNGCs was previously mentioned to reside at the amino terminus. In plant CNGCs, it has been reported that the CaMBD resides at the end of the CNBD or within CNBD (Schuurink *et al.*, 1998; Köhler and Neuhaus, 1998; Arazi *et al.*, 1999; Köhler and Neuhaus, 1999). A CaMBD located within the CNBD suggests that a cyclic nucleotide and a calmodulin may regulate this channel antagonistically. To support this notion, Ali *et al.* (2006) conducted a complementation analysis by heterologously expressing *ATCNGC1* lacking the CaMBD in the K^+-uptake deficient yeast (*trk1,2*) and *E. coli* mutants (which additionally lacks endogenous calmodulin). In this study, they showed the channel function was enhanced in *E. coli* but not in yeast when complemented with this truncated *ATCNGC1*, indicating the inhibition of channel function by yeast calmodulin.

Although some studies reported plant CNGCs can function as a homomer in various heterologous expression systems, based on the structural similarity to animal CNGCs, it is speculated that plant CNGCs also form heterotetramers *in planta*. However, by present, no study has been published about heterotetramerization of plant CNGCs.

1.3 Ion selectivity of CNGCs

Animal CNGCs are defined as non-selective cation channels because they do not discriminate between K^+, Na^+, and Ca^{2+} well (Zagotta and Siegelbaum, 1996). The pore of animal CNGCs contains a GETP sequence were there would be a GYGD sequence acting as a selectivity filter in channels selective for K^+ ions (Kaupp and Seifert, 2002). It is the GETP sequence which is believed to be responsible for the inability of animal CNGCs to discriminate between cations. There is neither a GETP nor a GYGD sequence in the pore of ATCNGCs. Instead, there is a conserved GQNL in 9 of the 20 ATCNGCs, which includes ATCNGC1, 3, 10, 11 and 12 (Figure 3) (Kaplan *et al.*, 2007). ATCNGC2 and 4 are both completely unique in terms of this ion selective filter by having the sequence of ANDL and GN-L, respectively. The differences in this selectivity filter sequence may provide plant CNGCs a unique ability to discriminate between ions more than animal CNGCs (Leng *et al.*, 1999; Hua *et al.*, 2003a; Gobert *et al.*, 2006; Borsics *et al.*, 2007).

A functional analysis of ATCNGC1, 2, 3, 4 and 10 in a heterologous system showed they could freely conduct K^+ (Leng *et al.*, 2002; Balague *et al.*, 2003; Hua *et al.*, 2003; Li *et al.*, 2005; Gobert *et al.*, 2006; Borsics *et al.*, 2007). However, only ATCNGC1, 3 and 4 allowed for Na^+ uptake (Leng *et al.*, 2002; Balague *et al.*, 2003; Hua *et al.*, 2003a; Gobert *et al.*, 2006). All of these functional analyses were performed in either mutant yeast strains lacking either their major Na^+ or K^+ channels or a mutant *E. coli* lacking the major K^+ channels.

When the yeast mutant strain WD3, lacking two major K^+-uptake transporters, *trk1, trk2* (Mercier *et al.*, 2004), expressed either *ATCNGC11* or *12*, the yeast was able to

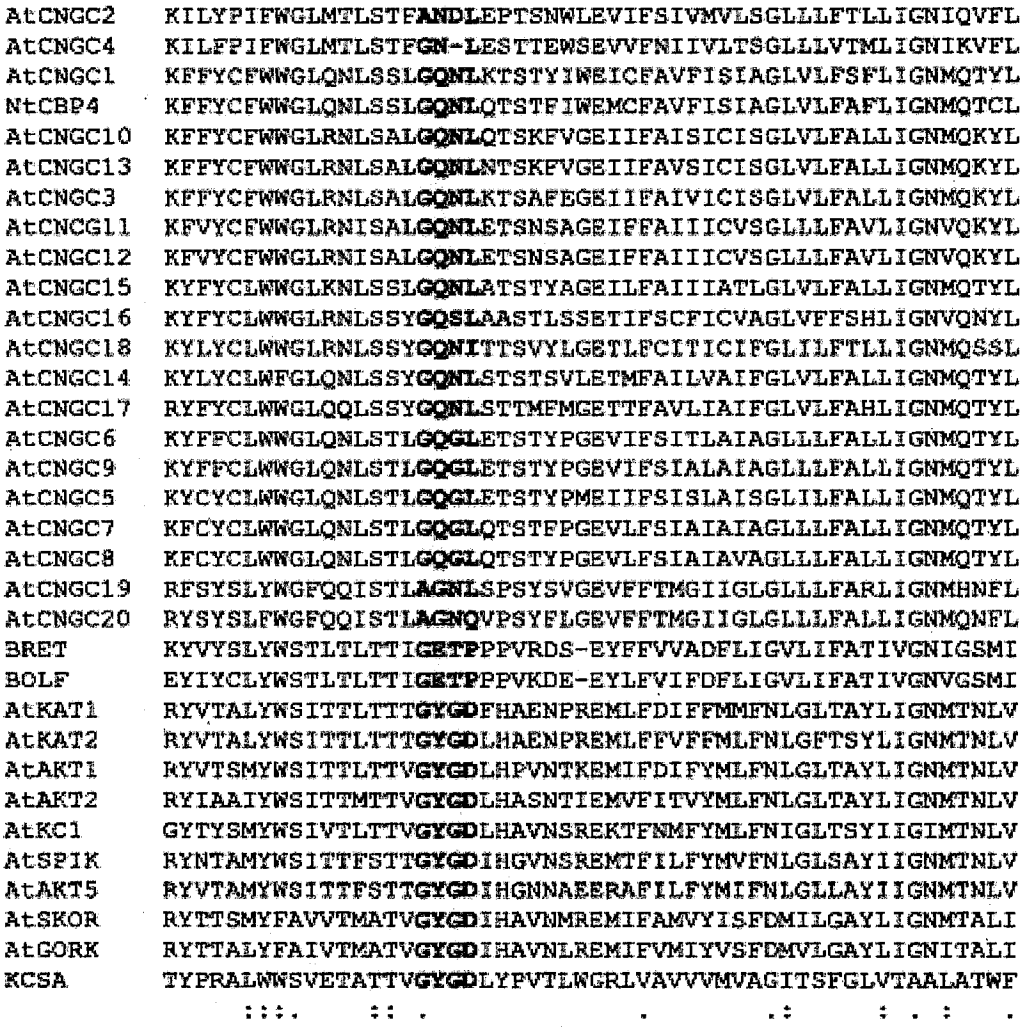

Figure 3. Taken from Kaplan *et al.*, (2007). Amino acid sequence alignment of the S6 and pore region of the 20 *Arabidopsis* CNGCs, the shaker-like K+-selective channels (AtKAT1 and 2, AtAKT1, 2 and 5, AtKCl, AtSPIK, AtSKOR, and AtGORK), tobacco (NtCBP4), bovine CNGCs (BRET and BOLF) and the *Streptomyces lividans* K+ channel (KCSA). The presumed selectivity filter is highlighted in red.

grow in K^+ minimal media indicating that both of these ATCNGCs are permeable to K^+ ions and can form homomeric functional channels *in vitro* (Yoshioka *et al.*, 2006). A similar result was obtained using a yeast mutant lacking its major Ca^{2+} channels indicating that they were also able to permeate Ca^{2+} ions (Urquhart *et al.*, 2007) unlike that of ATCNGC1 which was unable to permeate Ca^{2+} when expressed in the same yeast mutant (Ali *et al.*, 2006). The heterologous expression of ATCNGC18 in *E. coli* elevated the Ca^{2+} ion concentration inside the cells (Frietsch *et al.*, 2007)

1.4 The CNBD structure and key residues

Cyclic nucleotides are ubiquitous intercellular secondary messenger. It has been reported that many cellular processes are regulated by these small molecules through their effectors, such as protein kinase A and the Rap guanine nucleotide-exchange factor Epac (Rehmann *et al.*, 2007). Intracellular cyclic nucleotides have also been found to interact with animal CNGCs and induce gating (Yau and Baylor, 1989; Zagotta and Siegelbaum, 1996; Kaupp and Seifert, 2002). The CNBDs of a plant or animal CNGC share similarity in their protein sequence and structure to the CNBDs found in cAMP- and cGMP-dependent protein kinases, cAMP-dependent G-protein exchange factors, and the bacterial catabolite activator protein (CAP) (Arazi *et al.*, 2000; Kaupp and Seifert, 2002; Hua *et al.*, 2003b). CNBD sequences are also found in several other voltage and ligand-gated potassium channel family members that share homology to that of CNGCs, such as hyperpolerization-activated cyclic nucleotide-gated (HCN) "pacemaker" and ether-a-go-go (EAG) channels (Anderson *et al.*, 1992; Sentenca *et al.*, 1992; Robinson and Siegelbaum, 2003).

A reliable three-dimensional model for CNBDs was generated based on a crystal structure analysis of the CNBD within the CAP (Weber and Steitz, 1987). This model delineates a "roll subdomain" and a "C-helix subdomain" connected by a conserved proline also found in animal CNGCs (Figure 1). The roll subdomain consists of two α-helices, "A-helix" and "B-helix", which flank an eight-stranded β-barrel (β1 to β8). In between the sixth and seventh β-strand there is a short "P-loop" and "PB-loop". The C-helix subdomain consists of a single helix and in plant CNGCs the C-helix contains the CaMBD.

The overall structure of the β-barrel in the CNBD is similar in both plant and animal CNGCs. The β-barrel has a "jelly-roll"-like topography due to the eight β-strands, which make up two antiparallel β-sheets consisting of four strands each, causing the β-barrel to flatten (Kaupp and Seifert, 2002). A bound cyclic nucleotide can be held in this β-barrel by a number of polar and non-polar interactions. In the PB-loop between β6 and β7, the residues interact with the negatively charged phosphate and the ribofuranose moiety of a cyclic nucleotide through several hydrogen bonds and electrostatic contacts (Kaupp and Seifert, 2002). The residues from the β6 to the end of the β7 are therefore referred to as the phosphate binding cassette (PBC). Analysis of the ATCNGC2 CNBD through computational modeling identified three residues, G599, D600, and S619, which are predicted bind to the ribofuranose moiety and the phosphate in cAMP (Hua *et al.*, 2003b).

In animal CNGCs, the purine ring of cyclic nucleotides will interact with particular residues in the C-helix of the CNBD through hydrogen bonds (Zagotta and Siegelbaum, 1996). Previous studies using nucleotide analogs have demonstrated that the

C-helix is responsible for ligand selectivity (Goulding *et al.*, 1994). cGMP and cAMP are different only at the C_2 and C_6 positions of the purine ring (Figure 4). Therefore, various substitutions in the purine ring of cyclic nucleotides were created to test how the purine structure contributes to ligand selectivity (Tanaka *et al.*, 1989; Scott and Tanaka, 1995; Wei *et al.*, 1996; Scott *et al.*, 2000; Scott *et al.*, 2007). In these studies the alterations in its size and charge of the purine ring were reported to alter its ability to activate rod CNGCs. Contrary, alterations to the residues in the PBC in the CNBD will completely abolish channel activity in rod CNGCs (Scott *et al.*, 2007). Together, these studies suggest that the purine ring controls ligand selectivity and the ribofuranose stabilizes the ligand in the β-roll (Kaupp and Seifert, 2002).

1.5 Channel gating and subcellular localization

The C-linker region exhibits a unique tertiary structure in which there are no related structures currently in the protein data bank. Yet it has been reported that the C-linker plays a crucial role in the arrangement of the interacting subunits and gating of the tetrameric channels (Goulding *et al.*, 1994; Craven and Zagotta, 2004). The C-linker is thought to mediate most of the subunit-subunit interaction in HCN2 channels (Zagotta *et al.*, 2003). Also, the C-linker interacts with residues in the CNBD such that when a cyclic nucleotide binds to the β-barrel, a movement in the C-helix of the CNBD causes some movement in the C-linker (Matulef *et al.*, 1999; Taraska and Zagotta, 2007). A mutation to a residue that allows the C-linker and the CNBD to interact could disrupt the necessary stoichiometry for the correct subunit interactions.

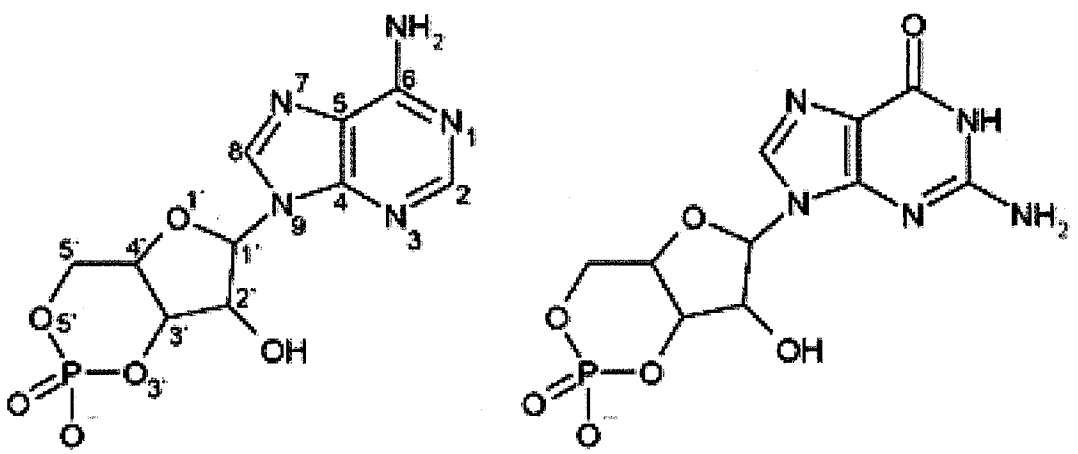

c - AMP **c - GMP**

Figure 4. Structure of cAMP and cGMP. A cyclic nucleotide molecule consists of a purine ring (adenine for cAMP or a guanine for cGMP) and a ribofuranose moiety with a phosphate that has formed hydrogen bonds between the C3 and C5 of the ribofuranose. The difference between cAMP and cGMP are at the C_2 and C6 position of the purine rings.

Mutations in the CNBD can also abolish channel activity, such as by causing improper subcellular protein localization. Several studies with *HCN2* and the *human ether-a-go-go-related* gene (*HERG*) have provided some evidence that the CNBD of CNGCs may be necessary for proper subcellular localization of these channels. *HERG* encodes a CNBD-containing K^+ channel found in cardiac tissue and abnormal HERG function is associated with ventricular arrhythmias and sudden death (Curran *et al.*, 1995; Sanguinetti *et al.*, 1995). Single point mutations in the CNBD or a truncation of the entire C-helix in the CNBD of HCN2 and HERG were reported not to affect the formation of tetramers and instead the channels were retained in the golgi apparatus and the ER, respectively (Akhavan *et al.*, 2005).

Localization of the tobacco CNGC, NtCBP4, (Arazi *et al.*, 1999), the barley CNGC, HvCBT1 (Schuurink *et al.*, 1998) and the *Arabidopsis* CNGCs, 10, 5, 3, 18, 11 and 12 and ATCNGC11/12 (Gobert *et al.*, 2006; Borsics *et al.*, 2007; Urquhart *et al.*, 2007; Frietsch *et al.*, 2007; Christopher *et al.*, 2007) has been observed in the plasma membrane. The localization of ATCNGC10 and 3 were shown in plant-based analyses and ATCNGC11, 12 and ATCNGC11/12 have been shown in yeast.

1.6 The *Arabidopsis cpr22* mutant

In prior work, the *Arabidopsis* mutant, *constitutive expresser of PR genes22* (*cpr*22) was isolated (Yoshioka et al., 2001, 2006). *cpr22* exhibits stunted growth with curly leaves and falls into a category of lesion mimic mutants with various constitutively active defense responses (Figure 5). *cpr22* displayed enhanced resistance to two distinct types of pathogens, the oomycete pathogen *Hyaloperonospora parasitica* isolate Emco5

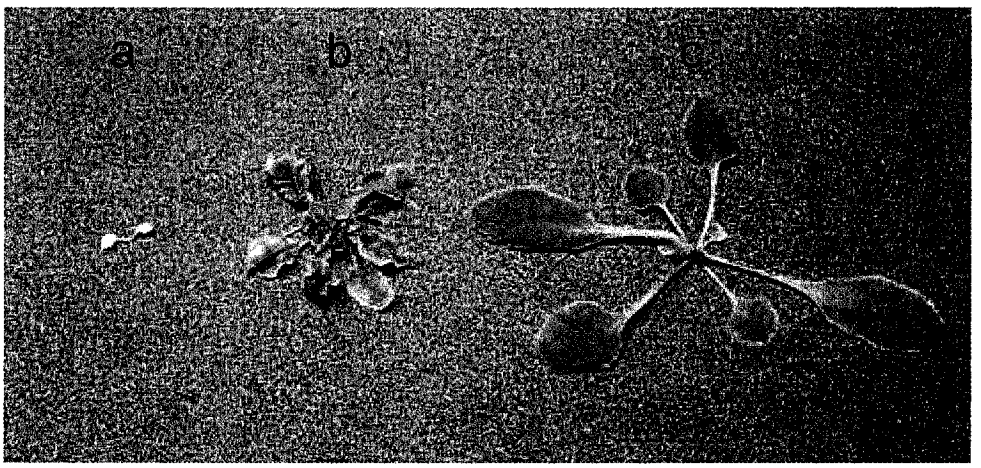

Figure 5. Morphological phenotype of the *Arabidopsis cpr22* mutant. (a) *cpr22* homozygous grown under ambient humidity. (b) *cpr22* heterozygous. (c) wildtype *Arabidopsis*.

and Emwa1 as well as the bacterial pathogen *Pseudomonas syringae pv.* maculicola ES4326 (Yoshioka *et al.*, 2001; Yoshioka *et al.*, 2006). Interestingly, these phenotypes are strikingly similar to that of the null mutants of *ATCNGC2* (*dnd1*) (Yu *et al.*, 1998; Clough *et al.*, 2000) and *ATCNGC4 (dnd2/hlm1)* (Balague *et al.*, 2003; Jurkowski *et al.*, 2004).

The *cpr, dnd* and *hlm* mutants fall into a class of *Arabidopsis* mutants that display constitutive *PR* gene expression, increased SA levels and a heightened resistance to virulent and avirulent pathogens. *cpr1, cpr5* and *cpr6* share all of these phenotypes with *cpr22,* however, it is only *cpr5* which also has spontaneous lesion formation (Bowling *et al.*, 1994, 1997; Clarke *et al.*, 1998, 2000). This spontaneous lesion formation in *cpr5* is SA-independent (Bowling *et al.*, 1997), whereas the morphological phenotypes and spontaneous lesion formation in *cpr22* are SA-dependent (Yoshioka *et al.*, 2006). Furthermore, *cpr6* has a similar morphological phenotype to *cpr22*, such that *cpr6* has stunted growth, which is also attributed by a SA-dependent pathway (Clarke *et al.*, 2000).

The SA-dependent pathway in *cpr22* is responsible for constitutive expression of the *PR-1* gene, stunted growth, spontaneous lesions, lethality in homozygous plants and enhanced resistance to *H. parasitica* (Yoshioka *et al.*, 2001). This was determined by crossing the *cpr22* mutant with the *Arabidopsis* mutant, NahG, which is carrying a transgene (*nahG*) that metabolizes SA into catechol. Furthermore, from crossing *cpr22* to *Arabidopsis* mutants that are non-expressors of *PR-1* (*npr1-5*) it was determined that the constitutive expression of *PR-1* in *cpr22* is *NPR1*-dependent (Yoshioka *et al.*, 2001). *npr1* mutants are insensitive to SA, fail to develop a HR and have a enhanced disease susceptibility (Cao *et al.*, 1994; Delaney *et al.*, 1995; Glazebrook *et al.*, 1996; Shah *et al.*,

1997). It was suggested that *NPR1* is an important factor downstream of SA accumulation in order to express *PR-1*. Therefore it was important to determine if *CPR22* functions in the same pathway as *NPR1*. The stunted growth, spontaneous lesions, lethality and enhanced pathogen resistance are all *NPR1*-independent (Yoshioka *et al.*, 2001). *cpr5* and *cpr6* plants demonstrate a similar resistance to *H. parasitica* that is also *NPR1*-independent (Bowling *et al.*, 1997; Clarke *et al.*, 1998). This data indicate that there is a signaling branch after SA accumulation and before *NPR1* to induce these phenotypes.

The enhanced pathogen resistance in *cpr22* is also mediated by an *R* gene-mediated signal transduction pathway that requires the resistance signal transducers *EDS1, PAD4*, and *NDR1* (Yoshioka *et al.*, 2006). The *Arabidopsis EDS1* and *PAD4* genes encode lipase-like proteins that are predominantly required by a particular *R* gene class with a N-terminal domain homologous with Toll and the interleukin-1 receptor followed by a nucleotide binding site and leucine-rich repeat (TIR-NBS-LRR) (Feys *et al.*, 2001). Contrary, another R gene class with a coiled-coil, NBS and LRR (CC-NBS-LRR), predominantly requires the *NDR1* for defense response (Aarts *et al.*, 1998). *NDR1* encodes for an integral membrane protein, yet the precise biochemical activity for NDR1 is not yet known (Century *et al.*, 1997). Analyses of double mutants, *cpr22/pad4, cpr22/eds1,* and *cpr22/ndr1,* demonstrated a loss of *cpr22*-conferred enhanced pathogen resistance but no change in elevated SA accumulation, stunted and curly-leafed plants, spontaneous lesions, or to the constitutive *PR-1* expression (Yoshioka *et al.*, 2006). This suggested that the heightened pathogen resistance in *cpr22* is not only SA-dependent but also both *NDR1*- and *EDS1/PAD4*-dependent.

cpr22 also has constitutive expression of the defensin gene, *PDF1.2*, which is a marker gene for the activation of jasomonic acid (JA) and ethylene signaling pathways. Double mutant analysis between *Arabidopsis* mutants which are defective in the JA (*coi1-1*) and ethylene (*etr1-1*) signaling pathways with *cpr22* demonstrated that the constitutive expression of *PDF1.2* is JA- and ethylene-dependent and SA-independent (Yoshioka *et al.*, 2001).

cpr22 was identified as a semi-dominant mutation that is lethal in the homozygous state unless the plant is grown under high relative humidity (>90%, Figure 5) (Yoshioka *et al.*, 2001). Recently, the *cpr22* mutation was identified as a 3-kb deletion that fuses two CNGC-encoding genes, *ATCNGC11* and *ATCNGC12*, to generate a novel chimeric gene, *ATCNGC11/12* (Figure 6) (Yoshioka *et al.*, 2006). Based on genetic, molecular and complementation analyses, it is suggested that ATCNGC11/12, as well as ATCNGC11 and ATCNGC12, form functional CNGCs and that the phenotype conferred by *cpr22* is attributable to the expression of *ATCNGC11/12* (Yoshioka *et al.*, 2006; Urquhart *et al.*, 2007).

Arabidopsis knockout lines for either *ATCNGC11* or ATCNGC*12* did not display the phenotypes conferred by *cpr22* but showed partially reduced resistance to the avirulent pathogen *H. parasitica* isolate Emwa1. This reduction in resistance suggests a role for ATCNGC11 and 12 in pathogen defense and that ATCNGC11/12 is constitutively activating defense responses, possibly by generating a downstream signal normally activated by ATCNGC11 or 12.

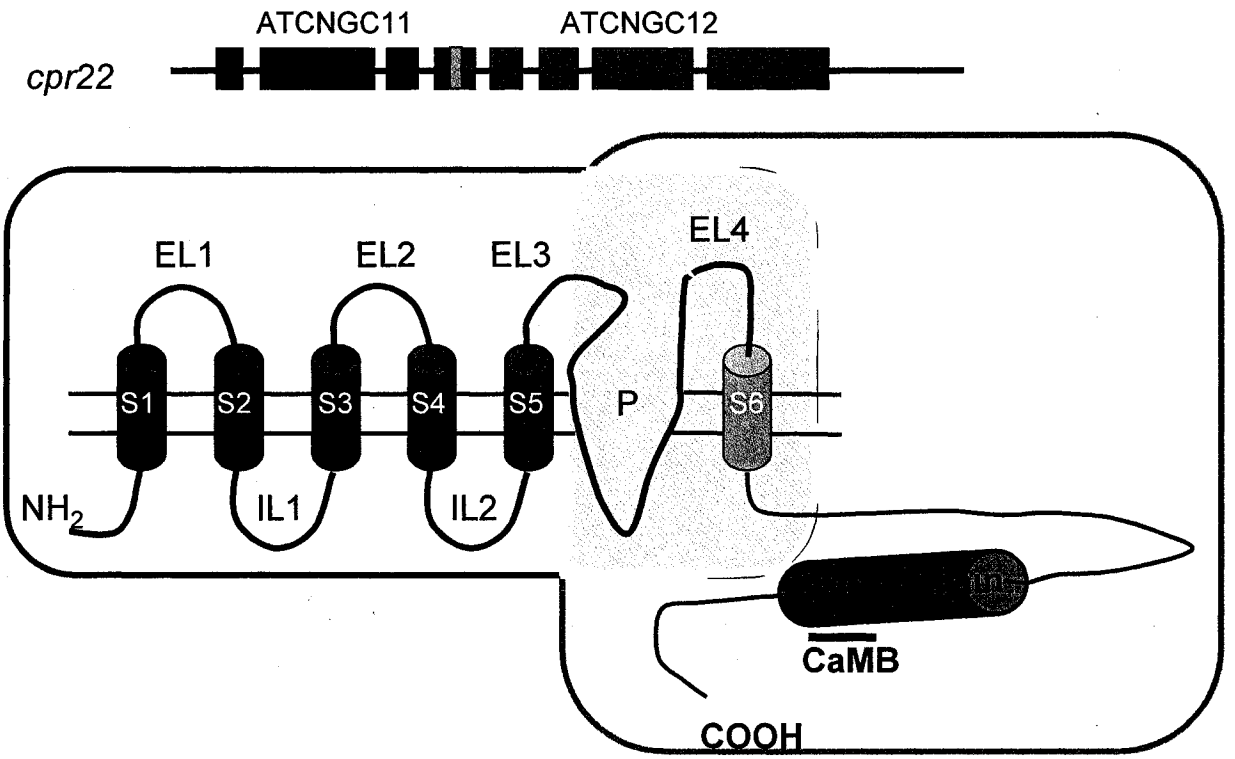

Figure 6. The chimeric gene, *ATCNGC11/12*, in the *cpr22* plant (above) and the protein model of the chimeric channel (below). The orange box delineates the portion of the channel contributed by ATCNGC11 and the brown box delineates the portion contributed by ATCNGC12. The portion in the yellow box has the exact same sequence in both ATCNGC11 and 12, and therefore it can not be determined which channel has contributed this portion. Legend: external loop (EL); internal (cytosolic) loop (IL); transmembrane segment (S1-S6); pore (P); cyclic nucleotide binding domain (CNB domain); calmodulin binding domain (CaMB).

Thesis objectives

The specific objectives of my thesis are: 1) to characterize the intragenic *cpr22* suppressor mutant #73, and 2) to investigate the molecular mechanism of the suppression of *cpr22*-related phenotypes by this mutation. This study aims to evaluate the possibility to use ATCNGC11/12 as a tool to identify the functionally important residues of CNGCs.

CHAPTER 2 – Methods and Materials

2.1 Growth conditions

All *Arabidopsis thaliana* seed lines were sown on PRO-MIX soil (Premier Horticulture Inc., Red Hill PA, USA) and stratified in the dark at 4°C for two days in order to synchronize germination. Seeds were germinated and grown under 16 hours of fluorescent light (45 μmol/m^2/sec) in a growth chamber that maintained a temperature of 22°C and a relative humidity (RH) of 55%; except those homozygous for *ATCNGC11/12* which were grown at a RH of 95%. *Nicotiana benthamiana* plants were grown on the same soil in the greenhouse under seasonal light and ambient humidity.

2.2 Plant material

A knock-out line for the *ATCNGC12* gene (KO12) was generated using the T-DNA insertion line SALK_092657 (ecotype Col-0) obtained from the SALK institute (Yoshioka *et al.*, 2006) and used along with a Ws wildtype (wt) plant to create the transgenic plant lines described in this thesis.

2.3 Suppressor screening and identification of the #73 mutant

The *Arabidopsis* plants used as a control line are of the Ws ecotype, unless otherwise noted. The *cpr22* mutant previously identified (Yoshioka *et al.*, 2001) is also of the Ws ecotype and therefore all suppressor lines for the *cpr22* mutant, including suppressor #73, are of the same ecotype. Approximately 10,000 *cpr22* homozygous seeds M_0 were mutagenized with 0.3% (v/v) ethylmethane sulfonate (EMS) solution (Sigma-Aldrich) for 8 hours at room temperature (RT), followed by rinsing with water more than 15 times. The M_0 seeds were grown under high RH of 95% for M_1 plants. Seeds from M_1

plants (M_2 seeds) were grown under ambient RH conditions to screen for suppressor plants. One of these plants, #73, which had the physical appearance of a Ws-wt plant, was identified through this screening. Suppressor #73 was then backcrossed with a homozygous *cpr22* plant for genetic analysis. The homozygosity of the *ATCNGC11/12* gene was confirmed by a PCR based marker (see the "General Molecular Biology" section for PCR conditions and Table 1 in Appendix for primer sequences, "D2DT_for" and "D2DT_rev").

2.4 General molecular biology

2.4.1 Media for bacterial cultures

See Appendix, Table 2, for a summary of the media for bacterial cultures.

2.4.2 Yeast Strains and Growth Conditions

The K^+ uptake-deficient *Saccharamyces cerevisiae* strain CY162 (*trk1,2*) (Gaber *et al.*, 1988; Ko and Gaber, 1991) was used for the channel complementation assay. The CY162 yeast was made competent first by growing it in YPD medium at 30°C shaking overnight. The overnight culture was diluted in 50 ml YPD (1% yeast extract, 2% peptone, 2% dextrose) to an OD_{600} of 0.4 and grown for an additional 2 hrs. The cells were collected at 6000 rpm centrifugation for 6 min at 22°C and resuspended in 40 ml of 1X TE. At this time the cells were competent and were aliquoted into individual 1.5 ml tubes at 200 µl per tube and immediately placed in liquid nitrogen and then placed into a -80°C freezer for later use. Competent cells were thawed on ice and pelleted by brief centrifugation. The supernatant was removed and the cells were resuspended in 200 µl of 1x LiAc/0.5x TE and incubated at RT for 30 min. The cells were pelleted by brief

centrifugation and resuspended in 300 µl of 1x LiAc/40% PEG-3350/1x TE, 100 µg of boiled and cooled sheared salmon sperm DNA, and 1 µg of plasmid DNA. The yeast was incubated at 30°C for 30 min and then put into a 42°C water-bath for 40 min with inversions every 10 min. The cells were briefly centrifuged and the supernatant was removed. The cells were washed 2x by 1 ml sterile ddH_2O and then resuspended in 1 ml of sterile ddH_2O. A small aliquot (~20 µl) of the yeast was spread onto SC-*ura* (minimal medium containing 2% glucose, 0.67% Yeast Nitrogen Base without amino acids) plates and incubated for 2 days at 30°C. Synthetic dropout media minus uracil was added to the medium for selection from the yeast following transformation. The yeast vector, pYES2® (Invitrogen), (*URA3* marker) was transformed alone or containing *ATCNGC11/12, ATCNGC12, ATCNGC11/12:E519K* or *ATCNGC12:E527K*. In addition, 100 mM of KCl was added to SC-*ura* media for growing transformed CY162 yeast. This protocol was adapted from Invitrogen™ "Small-Scale Yeast Transformation" (Catalog no. V825-20).

2.4.3 DNA extraction

All plasmids extractions from *Escherichia coli* strains were performed using an alkaline extraction protocol as described in Sambrook and Russell, 2001, or using the GenElute™ Miniprep Kit (Sigma). This kit and all other kits were used according to the manufacturer's protocols. Genomic DNA was extracted from *Arabidopsis* plants by selecting 1-2 small leaves and following the protocol (Quick DNA prep for PCR) as described in *Arabidopsis* laboratory manual (Weigel and Glasebrook, 2002).

From yeast, all plasmids were extracted by pelleting a 1 ml yeast culture grown for 2 days at 30°C and vortexing the pellet with 100 µl of lysis solution (2% Triton X-

100, 1% SDS, 100 mM NaCl, 10 mM tris-HCl, pH 8, and 1 mM EDTA). Following this, 100 µl of phenol/chloroform and 0.1 g of acid-washed glass beads were added. The samples were then vortexed at high speed for 2 min and centrifuged for 2 min at 13,000 rpm. The supernatant was transferred to a clean tube and precipitated with 250 µl of 100% EtOH for 5 min at RT. This was followed by another centrifugation at 13,000 rpm for 5 min. The supernatant was removed and the pellet was washed with 500 µl of 70% EtOH and then re-centrifuged at 13,000 rpm for 2 min. The supernatant was discarded and the pellet was air-dried and resuspended in 10 µl of ddH_2O.

2.4.4 DNA Restriction endonuclease digestion

Restriction endonucleases where purchased from Fermentas and all enzymatic reactions were carried out according to the manufacturer's recommendations. DNA fragments generated by restriction endonuclease digestion were separated on 0.8% agarose gels, and products of the correct size were cut out from the gel using a clean razor blade. The DNA was extracted from the gel by using the GenElute™ Gel Extraction Kit (Sigma) and this is referred to as "agarose-gel purification" in subsequent sections.

2.4.5 DNA Ligations

All ligations were carried out in 10 µl reactions using 1 µl (5 Units) of T4 DNA ligase and the companion ligation buffer both obtained from Fermentas. Reactions were incubated overnight in a 16°C waterbath.

2.4.6 Bacterial Transformations

Both chemically competent and electro-competent *E. coli* cells were made and used for transformations. For chemically competent cells ~100 ng (or 4 µl from a 10 µl ligation) of plasmid was added to the cells and then left on ice for 20 min followed by a 30 sec incubation in a 37°C water-bath and then another 5 min incubation on ice. As for the electro-competent cells 50-100 ng (or 1-2 µl from a ligation) of plasmid was added to the cells and chilled on ice for 5 min and then transferred to a chilled electroporation-cuvette and was electroporated in a BioRad MicroPulser™ at 2.5 kV using a 0.2 cm cuvette. Either chemical or electro-competent cells would then have 1 ml of LB added to the cells and then placed in a 37°C shaker at 250 rpm for 1 hr and plated onto LB agar plates containing the appropriate antibiotic selection and incubated overnight at 37°C.

Agrobacterium, strain GV3101 was used for stable transformation of *Arabidopsis*. The introduction of plasmids into *Agrobacterium* was performed by the same protocol that was used for *E. coli* electro-competent transformations. *N. benthamiana* and tobacco BY-2 cell transformations were performed using the *Agrobacterium* strain, GV2260. This strain was made chemically competent to introduce the desired plasmid into the *Agrobacterium*. However, transformation for GV2260 required a slightly different heat-shock method. After the plasmid DNA was added the cells were put into liquid nitrogen for five minutes and then kept for 25 min at 37°C. After adding 1 ml of LB to either strain and incubating at 37°C for 1 hr, the cells were plated on LB agar containing rifampicin plus the appropriate selection antibiotic and grown for 2-4 days at 28°C. Positive colonies were screened by PCR detection of the *ATCNGC11/12:E519K* gene using the primers #1 and #32 (see Appendix, Table 1) and confirmed by restriction digest with *Hind*III.

2.4.7 Polymerase Chain Reaction (PCR)

PCR reactions consisted of a 20 µl total volume for screening purposes or 40 µl for agarose gel purification of the PCR product. Each PCR reaction contained 50-100 ng of template DNA, 0.125 mM working concentration dNTPs (from a 1.25 mM stock mixture of dATP. dCTP, dGTP and dTTP) (Fermentas), 20 µmol of each primer (Invitrogen), 1x PCR buffer (0.2 M Tris pH8.0, 0.25 M NaCl, 25 mM EDTA, and 0.5% SDS) and one unit of *Taq* polymerase (Fermentas). A PCR reaction consisted of an initial 2 min denaturation step at 94°C, followed by 24 to 39 cycles consisting of a 30 sec denaturation step at 94°C, a 30 sec annealing step at 55-65°C (depends on the T_m of the primers), an extension step at 72°C for 20 sec to 2 min (30 sec for every 500 bp of expected product size) and a final step at 72°C for 10 min. PCR reactions took place in a MJ PTC-200 Peltier™ Thermocycler. All PCR products were run on 1% agarose gels except when screening for the homozygosity of suppressor #73, a 4% was used. Plants homozygous for *cpr22* would produce a 180 bp band versus the 160 bp and 180 bp bands for *cpr22* heterozygous plants and Ws-wt plants.

2.4.8 RNA extraction and electrophoresis

All RNA was extracted using the TRIzol® Reagent (Invitrogen) according to the manufacturer's instructions. For plant tissue, 1-2 medium leaves were used. Yeast cells were grown to a mid-log phase (OD_{600} = 0.5-0.7) and used. Leaves or yeast cells were frozen in liquid nitrogen first and leaf tissue was then ground using a sterile pestle before TRIzol® was added. Half the amount TRIzol® (500 µl) was added directly to the frozen yeast cells along with 100 µl glass beads (Sigma) and vortexed for 1 min the rest of the

procedure was carried out the same as for plant RNA extraction except that all other subsequent volumes were also halved.

All prepared RNA samples were run on a 1x MOPS-formaldehyde agarose gel following a standard method (Sambrook and Russell, 2001). Samples were boiled at 65°C in sample buffer (1x MOPS, 0.2 M formaldehyde, 0.6 M Formamide, and 0.6% EtBr) for 15 min and then cooled on ice for 5 min.

2.4.9 Reverse transcriptase (RT)-PCR

cDNA was generated by SuperScript™ II Reverse Transcriptase (Invitrogen) using total RNA and following the manufacturer's instructions. The cDNA was then used in a PCR reaction using the thermocycle previously described and under the same conditions as for PCR. The β-tubulin and the *ACT1* genes were used as a control for plant and yeast RT-PCR, respectively. *ATCNGC* gene specific primers were used to detect gene expression in *N. benthamiana* and yeast mutants (see Appendix, Table 1 for all primer sequences).

2.5 *PR-1* detection by Northern hybridization

PR-1 gene detection was performed as previously described (Kachroo *et al.*, 1995) using a previously designed and used probe (Yoshioka *et al.*, 2001)

2.6 Plasmid construction

The *ATCNGC11/12* cDNA was digested from the plasmid, pMBP3-*ATCNGC11/12* (minus the stop codon, plus a green fluorescence protein, smGFP, Yoshioka *et al.*, 2006, Urquhart *et al.*, 2007) with *Xho*I and subcloned into pBluescript®

(Stratagene). The #73 point mutation (G1555A), which creates the residue change E519K, was introduced into the cDNA of *ATCNGC11/12* while in pBluescript, through the QuikChange® Site-Directed Mutagenesis Kit (Stratagene). Oligiomer primers "cpr22#73_for" and "cpr22#73_rev" were designed (see Appendix, Table 1) and the procedure was carried out following the manufacturer's instructions. The pBluescript-*ATCNGC11/12:E519K* plasmid was sequenced and sub-cloned back into pMBP3 (Cambia) by digestion with *Xho*I. The re-ligation was confirmed by digestion with *Hind*III for insertion and correct orientation (see Appendix, Figure 1).

In order to obtain the cDNA, of *ATCNGC11/12:E519K* with a stop codon and without the smGFP, a PCR product using the primers #67 and #68 (see Appendix, Table 1) was used to amplify *ATCNGC11/12:E519K* from pMBP3. The forward primer introduced a *Bam*HI site at the 5'-end of the cDNA. An A-tail was added to the PCR product to allow for ligation into pGEM®-T Easy (Promega).

This *ATCNGC11/12:E519K* (with stop codon) in pGEM plasmid was subcloned into pYES2® by digesting both the plasmid and the pYES2 vector with *BamH*I and *Not*I. Other plasmids, pYES2 (empty vector), pYES2-*ATCNGC12* and pYES2-*ATCNGC11/12* were constructed as previously described (Yoshioka *et al.*, 2006). For the construction of pYES2-*ATCNGC12:E527K*, both pYES2-*ATCNGC11/12:E519K* and pYES2-*ATCNGC12* were digested by restriction enzymes *Mun*I and *Xba*I. The 550bp fragment from pYES2-*ATCNGC11/12:E519K* contains the *E527K* mutation and was agarose gel extracted along with the 7450 bp fragment from the pYES2-*ATCNGC12* so that these two pieces of DNA were ligated together to create pYES2-*ATCNGC12:E527K*. The summary of the construction of the yeast expression vector is shown in Appendix, Figure 2.

The CNBD portion (T1323 to G1950) of ATCNGC12 and ATCNGC11/12:E519K (T1299 to G1926) was expressed in *E. coli* (BL21-DE3). The *E. coli* expression vector, pET28a(+)® (Novagen, Madison, WI, USA) was used. To express the CNBD portion of ATCNGC12, the CNBD cDNA for *ATCNGC12* was obtained from pGADT7-*ATCNGC12* by *Eco*RI and *Xho*I digestion and sub-cloned into pET28a to create pET28a-*CNBD12*. Whereas pET28a-*CNBD11/12:E519K* was created using PCR to amplify the CNBD portion of *ATCNGC11/2:E519K* with the primers "WS14-*Eco*RI" and #37 (see Appendix, Table 1). This product was then digested by *Eco*RI and *Xho*I in order to create the appropriate restriction enzyme sites for sub-cloning into pET28a. The summary of the construction of the CNBD clones in pET28a vector is shown in Appendix, Figure 3.

2.7 *Agrobacterium*-mediated transient expression

ATCNGC11/12:E519K in pMBP3 was transformed into the *Agrobacterium* strain GV2260 which was then subsequently used to transiently express *ATCNGC11/12:E519K* in *N. benthamiana* along with *ATCNGC11/12*, and *ATCNGC12* as described in Sessa *et al.*, (2000). *Agrobacterium* carrying either of these CNGC cDNAs or that of the empty pMBP3 vector (final density of 0.2 OD_{600}) were used to syringe-infiltrate the underside of *N. benthamiana* leaves and monitor these areas for cell death 2 days post infiltration. All *Agrobacterium* was infiltrated in a 1:1 ratio with *Agrobacterium* carrying the tobacco etch virus (TEV) helper component proteinase (HC-Pro), in order to prevent gene silencing in *N. benthamiana* (Mallory, *et al.*, 2002). The expression of these genes was

confirmed by RT-PCR (see the section "Reverse transcriptase (RT)-PCR" under "General molecular biology").

2.8 Subcellular localization analysis

The localization of ATCNGC12, ATCNGC11/12 and ATCNGC11/12:E519K was attempted in several different systems using the same constructs used in the transient expression of *N. benthamiana*. A first attempt was in tobacco bright yellow (BY) -2 suspension culture cells. The BY-2 cells were transformed with the plasmids, pMBP3-*ATCNGC11/12-smGFP* and pMBP3-*ATCNGC11/12:E519K-smGFP* using particle bombardment and *Agrobacterium* transfection. The *Agrobacterium* was prepared as described in the "*Agrobacterium*-mediated transient expression" section. BY-2 suspension cultures were grown for 4 days in 4.3 g/L MS salts, 30 g/L sucrose, 100 mg/L Myo-inositiol, 255 mg/L KH_2PO_4, 0.2 mg/L 2,4-D, 1 ml/L Thiamine-HCl, pH 5. Cells were centrifuged for 5 min at RT and resuspended in transformation buffer (4.3 g/L MS salts, 30 g/L sucrose, 100 mg/L Myo-inositiol, 255 mg/L KH2PO4, 1 ml/L Thiamine-HCl, 0.25 M sorbitol and 0.25 M mannitol, pH 5). For 8 ml of BY-2 cells, 200 µl of *Agrobacterium* and 8 µl of Acetosyringone (from a stock of 4 mg in 1 ml EtOH) were gently mixed together and incubated at 28°C for 24, 48 and 72 hrs. At each time point the BY-2 cells were collected and gently centrifuged (1000 rpm, 1 min, 22°C). Cells were washed in BY-2 media and observed under the microscope.

Tungsten particles (microcarriers) were prepared for particle bombardment transformation of BY-2 cells by placing 100 mg of tungsten particles (M-17-Biorad) in a glass vial and heated to 180°C overnight. Microcarriers were transferred to a 1.5 ml tube

with isopropanol and sonicated at a duty cycle of 30% and an output of 2, at 10 sec interval pulses for a total of 3 min. The microcarriers were then incubated at RT for 15 min and centrifuged for 10 sec at 13000 rpm. After removing the supernatant, the microcarriers were washed in sterile ddH_2O and vortexed. The microcarriers were incubated for 1 min at RT and centrifuged as above. The washing and centrifugation was repeated once more and the microcarriers were finally resuspended in 1 ml of sterile 50% (v/v) glycerol and aliquoted into 5 µl samples.

A microcarrier sample had 2.5-5 µg of plasmid DNA added and mixed thoroughly. To each sample, 16 mM spermidine (Sigma) and 1 M $CaCl_2$ was added. The samples were vortexed for 3 min and centrifuged briefly. The microcarriers were resuspended in 100% isopropanol, vortexed and centrifuged as above. The supernatant was removed and microcarriers were then resuspended in 48 µl of isopropanol. A sample of the microcarrier bound with plasmid were added onto macrocarriers (Biorad) and allowed to sit at RT until all isopropanol evaporated. Coated macrocarriers were set into macrocarrier holders on top of the stopping screen (Biorad). Rupture disks (1350 psi-Biorad) were also washed in isopropanol and loaded into the retaining cap and tightly screwed onto the gas acceleration tube. BY-2 cells were plated on petrie dishes lined with Whatmann filter paper soaked with transformation buffer and placed into a chamber of unit (PDS-1000 Helium Biolostic Particle Delivery System-Biorad). Helium tank pressure was set to 1500 psi, and the vacuum was created to 25 inches of mercury to allow firing of the DNA at approximately 1300 psi. After releasing the vacuum the plates were removed, sealed and placed at 24°C in the dark overnight.

The following day the transformed BY-2 cells were fixed with transformation buffer and formaldehyde (1:1) and mixed on a rocker for 40 min at RT in the dark. The cells were washed four times with 1 ml of 1x PBS (for 1L: 8 g NaCL, 0.2 g KCl, 1.44 g Na_2HPO4, 0.24 g KH_2PO4) for 2 min, on the rocker in the dark. After the last wash the cells were resuspended in 1 ml of 1x PBS and 10 µl of pectolyase (from a 10 mg/ml stock) was added and the cells were incubated at 28°C for 2 hrs in the dark on a rocker. Cells were then washed three times with 1x PBS and then resuspended in 1 ml of 1x PBS and observed under the microscope.

Arabidopsis Ws-wt and KO12 (Col-0) were used for floral dip transformation of *ATCNGC12, ATCNGC11/12* and *ATCNGC11/12:E519K.* First bolts from the plants were cut off (approximately 6 weeks old) and after 2 or more bolts had grown the plants were vacuum-infiltrated with the *Agrobacterium* (strain GV3101) carrying the appropriate construct. Plants were placed on their side and covered with saran wrap and left at RT in the dark overnight. The following day the plants were stood erect and grown until seed pods were matured and ready for collection. These seeds are referred to as the T_1 generation. Positive transformants were identified by growing the T_1 seeds on soil with Wipeout™ since the pMBP3 plasmid carries a Basta (glufosinate ammonium) selection gene. Plants from the T_2 generation were screened under the microscope for GFP in the epidermis of the leaves.

We attempted *Arabidopsis* protoplasts transfection by following the protocol described in Yoo *et al.*, (2007). However, we were unsuccessful. Therefore, we decided to collaborate with Dr. N. Kato at the University of Louisiana. Protoplast isolation and transfection with 10 µg of plasmid (pMBP3-*ATCNGC12*-smGFP, pMBP3-*ATNCG11/12*-

smGFP, pMBP3- *ATCNGC11/12:E519K*-smGFP or a plasmid which expresses a plasma membrane-localized protein, GFP-SYP123, courtesy of Uemura *et al.*, 2004) was performed as described in Fujikawa and Kato (2007). No plasmid was added during the transfection procedure to the mock samples.

Transfected protoplasts were observed with Leica TCS SP2 spectral confocal microscope equipped with a 40x, 1.25 numerical apertures, oil immersion objective lens and a 500 nm excitation beam splitter. A pinhole size was 81 μm (Airy 1). A 488 nm argon laser at 25% power was used to excite GFPs. A slit window of a photon multiplier tube (PMT) was 500-600 nm. Each image was manually adjusted for the gains of the PMT to increase signal-to-background ratios of the images. Images were zoomed to 3.2 fold and an area of 512 x 512 pixels (117 x 117 μm) was scanned with a resolution of 0.23 μm.

2.9 Pathogen infection and Trypan Blue staining

Cotyledons of 7 to 10-day-old seedlings were inoculated with *Hyaloperonospora parasitica* isolates Emwa1 or Noco2 by applying a single drop of a 10^6 asexual conidiosporangia/ml. Inoculated seedlings were covered with plastic wrap to keep a high humidity and grown at 16°C under an 8 hr photoperiod. At 7 dpi plants which displayed sporangiophore growth on the cotyledon surface were scored as susceptible. Leaf samples from plants after 7 dpi were taken to stain for sporangiophores in susceptible plants or dead cells using Trypan Blue staining was preformed as described in Yoshioka *et al.*, 2001.

2.10 Yeast complementation assay

The complementation assay was performed by growing the K^+ up-take deficient yeast mutant (*trk1,2*) strain CY162 carrying *ATCNGC11/12, ATCNGC12, ATCNGC11/12:E519K, ATCNGC12:E527K* or empty pYES2 vector (from a glycerol stock) in SC-*ura* media with 0.1 mM KCl. The cultures were grown at 28°C for 48 hours and the growth was recorded at 0, 24 and 48 hrs by measuring the OD_{600} with a spectrophotometer.

2.11 Protein expression in *E. coli*

The pET28a constructs carrying the CNBD domain of *CNBD12* or *CNBD11/12:E519K* were transformed into electro-competent *E. coli* strain BL21 (DE3) and selected on LB medium plus kanamycin plates for positive colonies. A positive colony was grown in a 1 L LB medium plus kanamycin culture to an OD_{600} of approximately 0.6, cooled on ice to approximately 4°C and then induced with 1 mM IPTG, as recommended for the pET28a vector under the T7 promoter. The induced culture was then grown overnight at 16°C. All proteins were extracted from the cells using a lysis buffer volume (150 mM NaCl, 0.5% NP40, 5 mM EDTA pH 5.0, and 10 mM Tris pH 7.5), and sonication (duty cycle of 90, output of 5) for 10 min (30 sec on / 30 sec off) and the CNBD12 or CNBD11/12:E519K recombinant proteins were purified from other contaminating proteins using Ni-NTA affinity chromatography. Fractions were pooled together and dialyzed overnight at 4°C in 50 mM Tris pH 7.5, 150 mM KCl, 5 mM $MgCl_2$, and 1 mM DTT. All proteins were stored at 4°C.

2.12 Protein conformation by Western blot analysis

The protein extracts were boiled in a 2x SDS loading buffer (in 1 ml: 100 µl 1.5 M Tris-HCl, pH 6.8, 60 µl 20% SDS, 300 µl glycerol, 150 µl β-mercaptoethanol, and 0.002mg Bromophenol Blue) for 2 min and run on a 12% SDS-PAGE gel at 130 mV in a Tris-glycine-SDS running buffer. The gels were then blotted onto a PVDF membrane (Millipore) at 150 mV in the appropriate buffers as directed by the manufacture of the electroblotting system (ThermoFisher Scientific). The proteins blotted to the membrane were probed with a His antibody (BIOSHOP, 1:2,500 dilution) and then with an α-rabbit antibody conjugated to horse radish peroxidase (Cell Signaling Technology, 1:2,500 dilution). Using the Western Lightning reagent Plus (Perkin Elmer, Shelton, CT, USA) cross-reacting protein bands were detected following the manufacturer's protocol.

2.13 CNBD assay

Agarose beads coated with cAMP (Sigma) were resuspended in 1 ml of buffer (50 mM Tris pH 7.5, 150 mM KCl, 5 mM $MgCl_2$, and 1 mM DTT) and 50 µl of this resin was incubated with 250 µg of either purified protein CNBD12 or CNBD11/12:E519K for 2 hrs at 4°C. The beads were concentrated and the supernatant was collected ("unbound" protein). The beads were then washed three times with the CNBD assay buffer (200 µl was used for the first wash and 500 µl was used for subsequent washes). The beads were then mixed with 50-100 µl of a 2x SDS-loading buffer and boiled for 5 min. Each sample (input, supernatant, first wash and bound protein) was run on a 12% SDS-PAGE gel and used for Western blotting to detect the His-tag. Competition assays followed the same

protocol except that, first, 10 μmol of either cAMP or cGMP was incubated with the CNBD protein for 20 min at 4°C and then the cAMP agarose beads were added.

2.14 Bioinformatics Analysis

A bioinformatics approach was taken to address the secondary and tertiary structure of ATCNGC11/12. Using the secondary structure prediction tool PHYRE (McDonnell *et al.,* 2006; www.sbg.bio.ac.uk/phyre/html/index.html) residue E519 in ATCNGC11/12 was found to be located in the eighth β-sheet of the CNBD. In a collaboration with the Christendat lab, University of Toronto, Cell and Systems Biology Department, the amino acid sequence of the cytosolic c-terminus domain from ATCNGC11/12 was modeled to the crystallized structure of the cytosolic c-terminus of HCN2 (PDB# 1Q50) using PYMOL (DeLano, W.L., 2002). The same portion of ATCNGC12 was modeled to the crystallized structure of the CNBD from RIα (PDB# 1NE6).

Multiple sequence alignments of the CNBD amino acid sequences of all 20 *Arabidopsis* putative CNGCs were aligned using the ClustalW alogthrim (Thompson *et al.,* 1994). Full length protein sequences for these CNGCs were obtained from the Entrez protein database (NCBI, http://www.ncbi.nlm.nih.gov/): AtCNGC1 (gi 38502855), AtCNGC2 (gi 38502856), AtCNGC3 (gi 18407073), AtCNGC4 (gi 38503128), AtCNGC5 (gi 42573714), AtCNGC6 (gi 38502863), AtCNGC7 (gi 15219100), AtCNGC8 (gi 15223667), AtCNGC9 (gi 15234769), AtCNGC10 (gi 38503202), AtCNGC11 (gi 79577669), AtCNGC12 (gi 3850303), AtCNGC13 (gi 38503199), AtCNGC14 (gi 38503238), AtCNGC15 (gi 3850324), AtCNGC16 (gi 38503242),

AtCNGC17 (gi 38503044), AtCNGC18 (gi 38503201), AtCNGC19 (gi 15229093), AtCNGC20 (gi 38503198). Other putative CNGCs from barley (gi 66933082), rice (gi 77555620), bean (gi 24943196) and tobacco (gi 6969231) homologs obtained from the blast search were aligned to the CNBD12. Human ion channels HCN2 (gi 156071470), CNGA1 (gi 71143141), and CNGA3 (gi 4502917) was aligned to the CNBD12 and ATCNGC11/12:E519K.

CHAPTER 3 - Results

3.1 Screening for suppressor mutants of *cpr22*

To identify downstream components of *cpr22 (ATCNGC11/12)*-mediated pathogen resistance signaling or to gain insight into the structural-functional relationship of ATCNGC11/12, a suppressor mutant screen was conducted. In this screen, we took advantage of the conditional lethal phenotype of *cpr22* homozygous plants under ambient humidity condition (Yoshioka *et al.*, 2001). c*pr22* homozygous seeds were treated with EMS and M_1 seeds were grown under high humidity conditions (RH95%). The M_2 generation was grown under ambient humidity conditions to identify mutants that exhibit suppression of the conditionally lethal phenotype of *cpr22.* Seventy-four plants survived under this condition and were classified into 6 groups based on morphological phenotype: 1) identical to wildtype, 2) similar to wildtype plus wavy leaves, 3) similar to *cpr22* heterozygous plants, 4) more pronounced phenotype than *cpr22* heterozygous, 5) identical to wildtype plus spontaneous lesion formation, and 6) others (Figure 7). Suppressors in Group VI ("Others") mainly consisted of three phenotypes: i) small plants with enhanced curly leaves that created a "star-like" leaf shape and HR-like lesions, ii) large plants with abnormal HR-like lesions which were much larger and created white patches on the leaves, and iii) small plants of a much lighter green tissue colour.

3.2 Identifying suppressor #73

Suppressor #73 is a plant from Group I that is morphologically identical to wildtype plants (Figure 8). Suppressor #73 has not only lost the conditional lethality of the *cpr22* mutation but has also lost the spontaneous lesion formation and constitutive

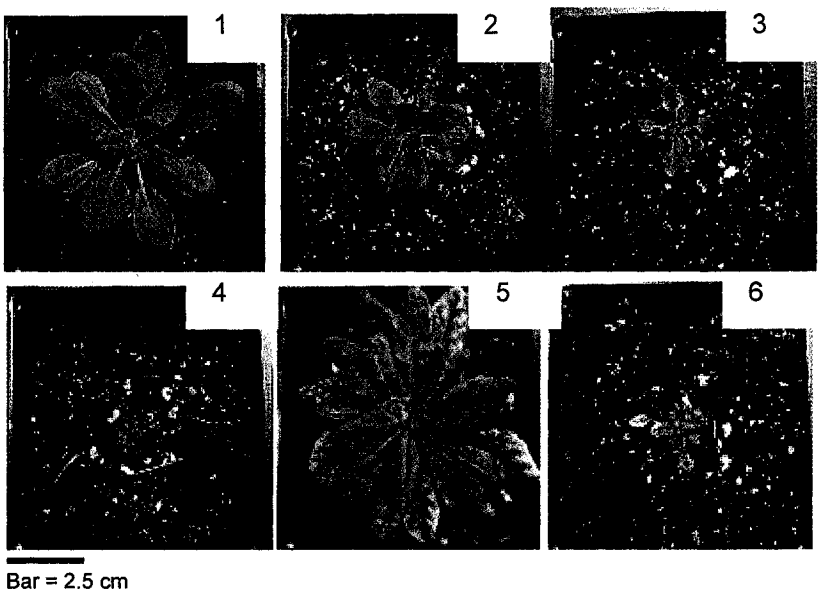

Figure 7. Representatives of the morphological phenotypes of the six groups of potential *cpr22* suppressors. All plants are five weeks old. Group 1: wildtype, Group 2: Similar to wildtype plus wavy leaves, Group 3: Similar to *cpr22* heterozygous plants, Group 4: More pronounced phenotype than *cpr22* heterozygous, Group 5: Identical to wildtype plus spontaneous lesion formation, and Group 6: Others. Picture courtesy of Kim Chin.

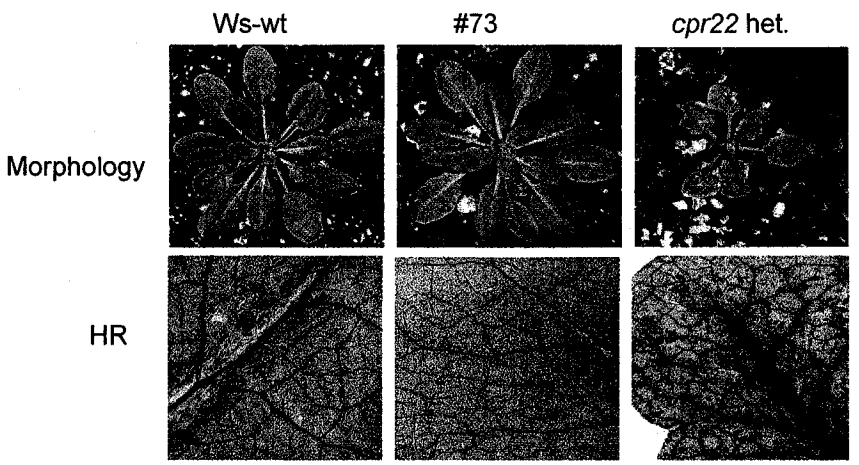

Figure 8. Morphological phenotype comparison of suppressor #73 to *cpr22* heterozygous (het.) and Ws wildtype (Ws-wt) *Arabidopsis* plants. Top panel: morphological phenotype. Bottom panel: Trypan Blue stain for dead cells which can only be seen in the images of *cpr22*.

expression of the *PR-1* gene (Figure 8 and 9). To evaluate the genetic nature of the #73 mutation, a backcross with *cpr22* homozygous plants which were grown in high humidity was carried out. As shown in Table 1, all B_1 (backcross first generation) plants showed *cpr22* heterozygous-like phenotypes, suggesting that the #73 mutation is semi-dominant, just as the original *cpr22* mutation itself. The following B_2 generation after self-pollination showed a segregation of; 1 (wildtype-like): 2 (*cpr22* heterozygous-like): 1 (lethal), further confirming the semi-dominant nature of this mutation (Table 1).

In order to confirm that this mutation was causing the *cpr22* suppression, and not a contamination from heterozygous or wildtype seeds, a PCR-based analysis was then conducted to ensure that its background is homozygous for *ATCNGC11/12*. By this analysis, wildtype and heterozygous *cpr22* plants show two bands (160 bp and 180 bp) and *cpr22* homozygous shows one band (160 bp). As shown in Figure 10, #73 has only one 160 bp band, indicating that it is homozygous in terms of *ATCNGC11/12*. Therefore, #73 is not a contamination. (Note: In the Ws-wt lane of Figure 10 there appears to be a third band slightly larger than the expected 180bp band. This band is only observed when wildtype genomic DNA is used for the PCR reaction. At this time, we are unable to explain the reason for this unexpected band and we are currently investigating the possible reason. However, sequencing confirms that the other expected band sizes are correct and therefore this PCR analysis is reliable to distinguish plants with a *cpr22* homozygous background.)

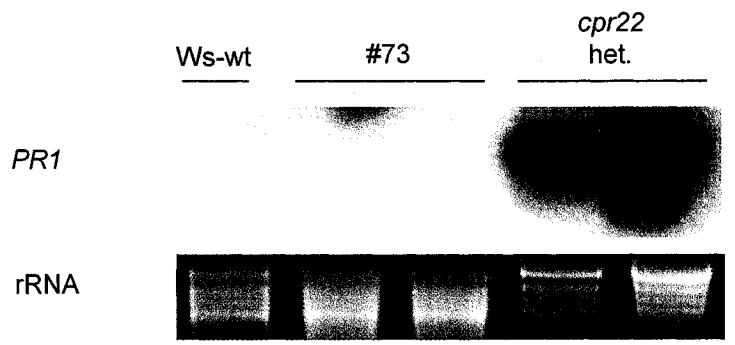

Figure 9. *PR-1* gene expression analysis in suppressor #73 by northern blot. *cpr22* heterozygous (het.) is a positive control and Ws wildtype (Ws-wt) is a negative control. rRNA is a loading control.

Table 1. Segregation of the *cpr22* morphological phenotype in suppressor #73 backcrosses.

		Morphological Phenotype						
Plant Line		Total No.	Wt	*cpr22*	lethal	Hypothesis[b]	X^{2c}	P
cpr22/CPR22		139	35	65	39	1:2:1	0.81	0.7>P>0.5
#73 x *cpr22/cpr22*	F_1	13	0	13	0	0:1:0	——	——
	F_2	111	25	59	27	1:2:1	0.51	0.8>P>0.7

[a] #73 is the pollen accepting plant
[b] Both *cpr22* and #73 are semi-dominant
[c] Two degree of freedom

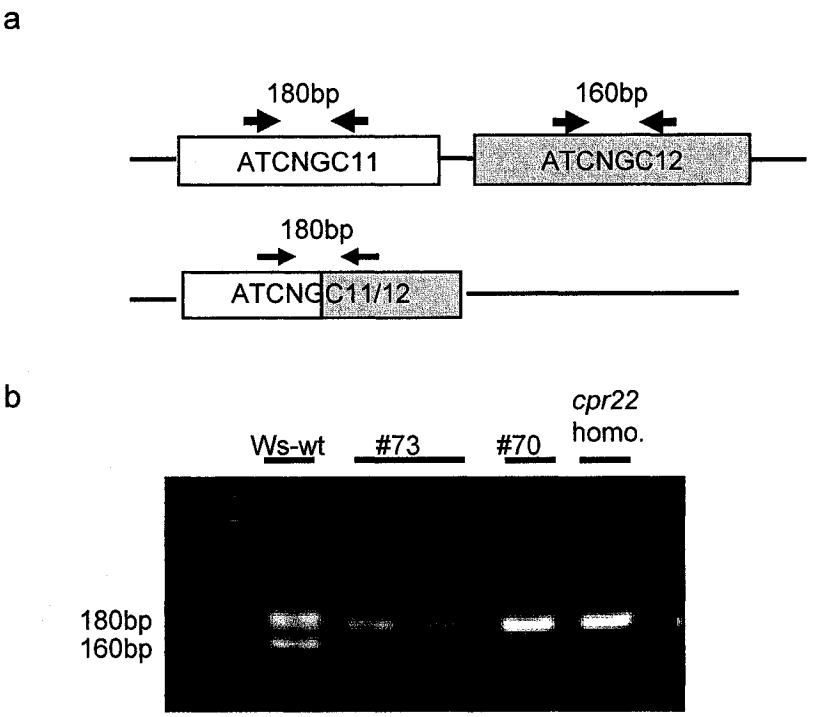

Figure 10. PCR analysis to confirm the *cpr22* homozygous background. (a) Diagram of how the primer position (arrows) and the expected PCR product sizes. (b) Plants with *cpr22* homozygous (homo.) background will have only one band of 180 bp, whereas Ws wildtype (Ws-wt) (or *cpr22* heterozygous) plants display both 160 bp and 180 bp bands . Suppressors #73 and #70 confirm the *cpr22* homozygous background. (Note: see the results section to explain the reason for a third band in Ws-wt lane)

3.3 Suppressor #73 is an intragenic mutant of *cpr22*

Since *cpr22* is a semi-dominant mutation, it indicated that the #73 mutation might be an intragenic mutation. This prediction led us to sequence the *ATCNGC11/12* gene in #73 plants. As shown in Figure 11, sequence analysis revealed that there is a nucleotide change, G1555A, in the CNBD. This point mutation caused an amino acid change: a glutamate (E) to a lysine (K) (Figure 11). This mutation is referred to as "E519K" because it occurred at the 519th residue and the chimeric channel ATCNGC11/12 with this mutation is referred to as ATCNGC11/12:E519K. The expression of *ATCNGC11/12:E519K* in suppressor #73 was then confirmed by semi-quantitative RT-PCR analysis. As shown in Figure 12, the amount of expression is comparable to that of the *ATCNGC11/12* gene in *cpr22* homozygous plants (when compared to the loading control), suggesting that the suppression of the *cpr22* phenotype is not due to the alteration of expression of this gene.

3.4 Loss of *cpr22*-mediated pathogen resistance in suppressor #73

Since the *PR-1* gene is a marker for SA accumulation and SA accumulation is often correlated to pathogen resistance, a loss of constitutive expression of *PR-1* gene suggested that suppressor #73 would also have lost the heightened pathogen resistance found in *cpr22. cpr22* is resistant to the isolates Emco5 and Emwa1 of the oomycete pathogen, *Hyaloperonospora parasitica* (Yoshioka *et al.*, 2001, 2006). However, these isolates are virulent to *Arabidopsis* Ws-wt and will therefore cause an infection in these plants. Pathogen resistance of suppressor #73 was evaluated using one of these virulent strains, Emwa1. As shown in Table 2 and Figure 13, the same degree of infection was

```
CNGC1       FCGEELLTWALDPHSSSNLPISTRTVRALMEVEAFALKADDLKFVASQFRRLHSKQLRHT
CNGC10      FCGEELLTWALDPHSSSNLPISTRTVRALMEVEAFALKADDLKFVASQFRRLHSKQLRHT
CNGC13      FCGEDLLTWALDPQSSSHFPISTRTVQALTEVEAFALAADDLKLVASQFRRLHSKQLQHT
CNGC3       FCG-DLLTWALDPLSS-QFPISSRTVQALTEVEGFLLSADDLKFVATQYRRLHSKQLRHM
CNGC11      SCG-DLLTWALYSLSS-QFPISSRTVQALTEVEGFVISADDLKFVATQYRRLHSKQLQHM
CNGC12      ICGELLFNGSR-------KPTSTRTVMTLTEVEGFILLPDDIKFIASHLNVFQRQKLQRT
#73         ICGELLFNGSR-------KPTSTRTVMTLTKVEGFILLPDDIKFIASHLNVFQRQKLQRT
```

Figure 11. Amino acid sequence alignment from group I of the *ATCNGC* gene family covering the area over the CNBD which contains the residue change found in suppressor #73 (in bold), E527K. Performed using ClustalW (Thompson *et al.*, 1994).

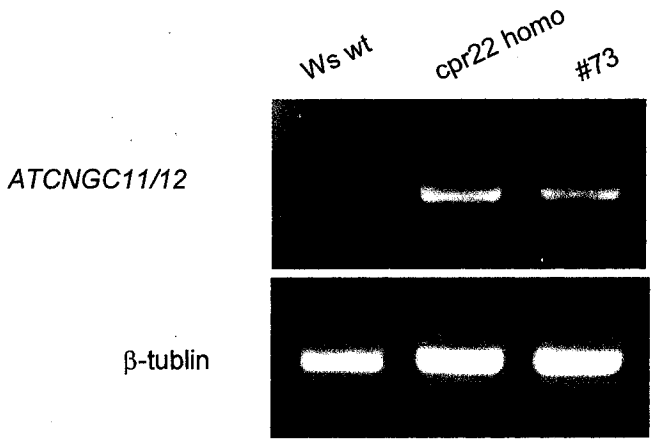

Figure 12. Gene expression analysis of *ATCNGC11/12* by RT-PCR. cDNA from *cpr22* homozygous, wildtype WS plants and suppressor #73. β-tublin represents a loading control.

Table 2. Interaction phenotype with *H. parasitica* isolate Emwa1

Plant	Total # of plants	# of plants[a]	
		R	S
Ws	28	3	25
cpr22/CPR22	21	21	0
Suppressor #73	30	0	30

[a] Based on formation of sporangiophores; R, no formation; S formation

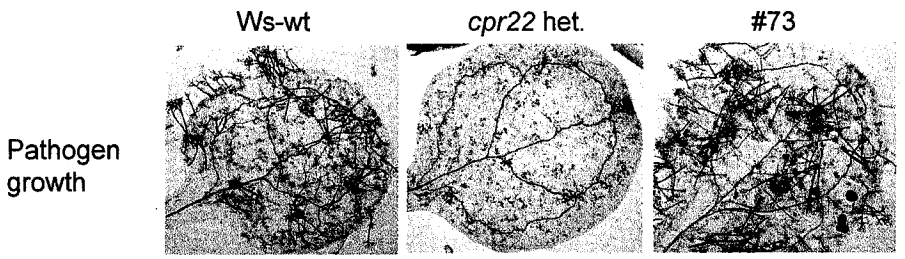

Figure13. Growth of *H. parasitica* isolate Emwa1 on Ws wildtype (Ws-wt), *cpr22* heterozygous (het.) and suppressor #73. Plants were infected by spraying a conidiospore suspension of 10^6 ml^{-1} on 7-d-old plants. The infected cotyledons were harvested 7 dpi and stained with Trypan Blue to visualize pathogen structures.

observed in suppressor #73 as in wildtype plants. Contrary, no pathogen growth was observed on *cpr22* plants. This experiment was repeated several times with similar results.

The same type of experiment was conducted using a different isolate, Noco2. Noco2 is an avirulent strain to the *Arabidopsis* Ws ecotype. Therefore, using this strain we can evaluate if the E519K mutation caused enhanced susceptibility to this pathogen. Since the #73 plant lacks wildtype *ATCNGC11* and *12* genes and the E519K mutation suppresses *ATCNGC11/12* function, #73 could be a potential double knockout of *ATCNGC11* and *12*. Since Yoshioka *et al.*, (2006) have suggested a positive role of these genes for pathogen resistance responses, it is interesting to analyze the pathogen resistance in this potential double knockout plant (#73). However, as shown in Table 3, suppressor #73 did not appear to have higher susceptibility to this avirulent strain of *H. parasitica.*

3.5 *ATCNGC11/12:E519K* abolishes the induction of HR cell death in *N. benthamiana*

The loss of all *cpr22*-associated phenotypes in suppressor #73 suggests that the E519K mutation caused this suppression. However, since EMS can cause multiple mutations, there is a possibility that another mutation in the genome suppresses the *cpr22*-mediated phenotypes in #73 plants. To confirm the significance of the E519K mutation, the same point mutation (GAA to AAA) causing E519K was artificially created in *ATCNGC11/12* by site-direct mutagenesis. This construct (ATCNGC11/12:E519K) was then tested for its ability to cause programmed cell death (PCD) in *Nicotiana*

Table 3. Interaction phenotype with *H. parasitica* isolate Noco2

Plant	Total # of plants	# of plants[a]	
		R	S
Col.	22	9	13
Ws	28	26	2
cpr22/CPR22	27	25	2
Suppressor #73	26	25	1

[a] Based on formation of sporangiophores; R, no formation; S formation

benthamiana using *Agrobacterium*-mediated transient expression. This method has been well established to observe PCD or HR-like cell death (Sessa *et al.*, 2000). It was previously used to determine if the expression of *ATCNGC11/12* is responsible for the HR-like cell death seen in *cpr22* and not the loss of *ATCNGC11* or *12* (Yoshioka *et al.*, 2006; Urquhart *et al.*, 2007). As shown in Figure 14a, transient expression of *ATCNGC11/12* caused clear HR-like cell death on *N. benthamiana* leaves, whereas expression of *ATCNGC11/12:E519K* did not induce cell death. Expression of *ATCNGC12* and the empty vector also did not induce cell death. The expression of *ATCNGC11/12* and *ATCNGC11/12:E519K* was confirmed visually by green fluorescence at the cell periphery from a GFP (green fluorescence protein) tag fused to the C-terminus of each protein as well as by RT-PCR (Figure 14b and 14c). Taken together, we concluded that the E519K mutation in suppressor #73 is responsible for the suppression of *cpr22* phenotypes.

3.6 The *E519K* mutation does not alter the subcellular localization of ATCNGC11/12

The observed GFP fluorescence in the periphery of the *N. benthamiana* cells after transient expression of *ATCNGC*s indicates that they are located in the plasma membrane. Furthermore, the studies of other ATCNGCs, animal CNGCs, HCN and HERG channels also indicates a localization in the plasma membrane (Zagotta and Siegelbaum, 1996; Akhavan *et al.*, 2005; Gobert *et al.*, 2006; Borsics *et al.*, 2007; Urquhart *et al.*, 2007). However, some mutations in the CNBD of HCN and HERG channels prevented proper subcellular localization (Akhavan *et al.*, 2005). Because the

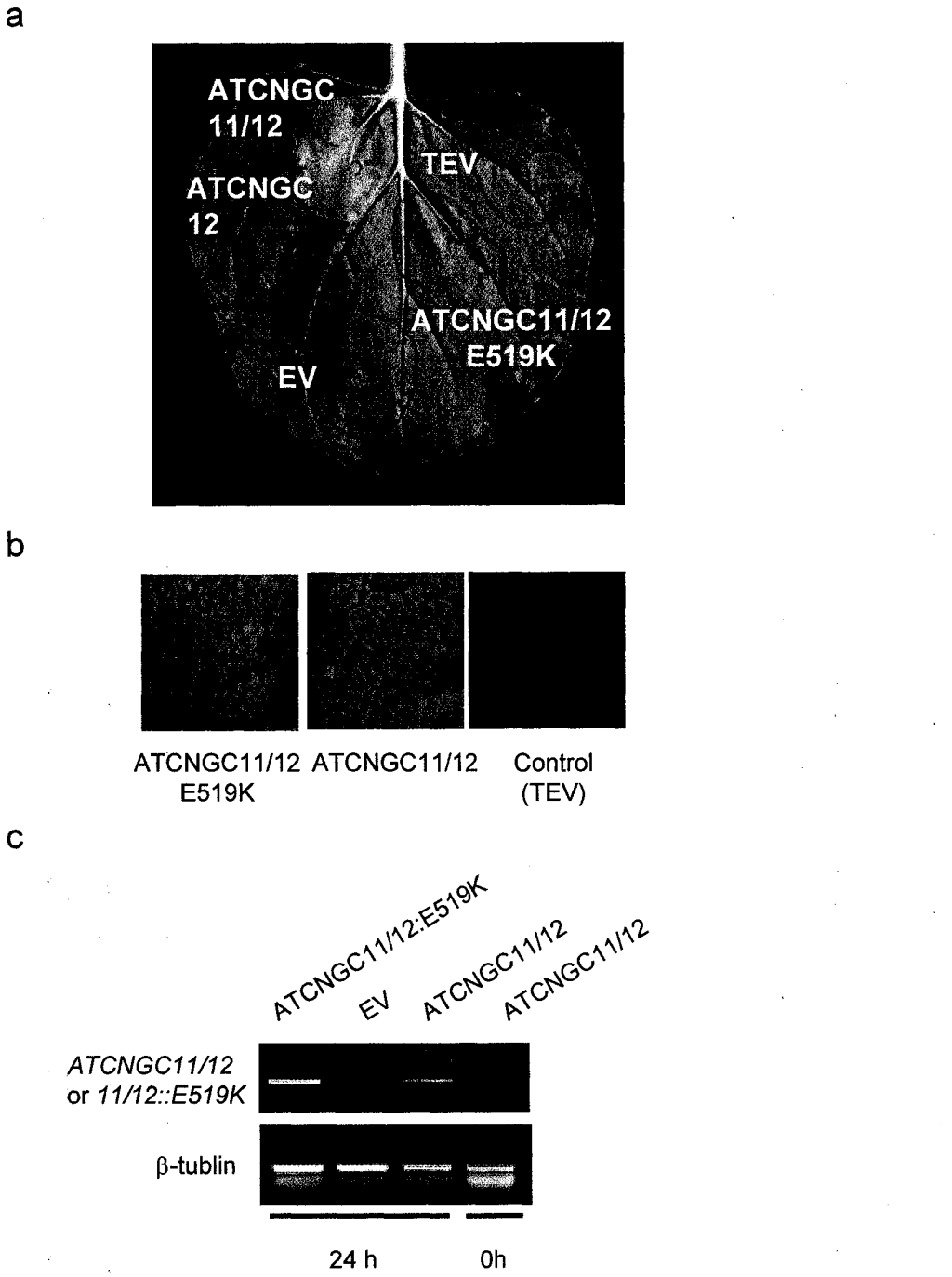

Figure 14. Transient expression of *ATCNGC12*, *ATCNGC11/12*, or *ATCNGC11/12:E519K* in *N. benthamiana*. (a) *Agrobacteria* containing an empty vector (EV - pMBP3) or a vector containing *ATCNGC12*, *ATCNGC11/12*, or *ATCNGC11/12:E519K* driven by the CaMV 35S promoter were infiltrated into *N. benthamiana* leaves. *Agrobacterium* carrying a component of the tobacco etch virus (TEV) was also used as a negative control (Note: the TEV component is used in all of the infiltrations, see Methods and Materials). The infiltrated areas are circled. Leaves were photographed at 48 hrs after infiltration and showed lesion formation only with *ATCNGC11/12* expression. Lesion formation is no longer present in leaf tissue infiltrated with *ATCNGC11/12*:E519K. (b) fluorescence from smGFP-fusion tag in the expressed consturcts. (c) Expression analysis of *ATCNGC11/12* or *ATCNGC11/12:E519K* by RT-PCR. cDNA was prepared from leaf areas infiltrated with *ATCNGC11/12* at 0 hrs and 24 hrs. cDNA for *ATCNGC11/12:E519K* and the EV were also prepared at 24 hrs.

E519K mutation is also in the CNBD, the possibility that this mutation prevents proper localization of ATCNGC11/12 can not be ruled out.

We have attempted to determine the localization of ATCNGC12, ATCNGC11/12 and ATCNGC11/12:E519K by several different approaches using GFP tagged proteins. However, despite many attempts, we did not obtain a conclusive result. Therefore, we have established a collaboration with Dr. Naohiro Kato's laboratory at the University of Louisiana. By this collaboration, we showed the localization of ATCNGC11, 12 and ATCNGC11/12 and ATCNGC11/12:E519K in the plasma membrane of *Arabidopsis* protoplasts (Figure 15). These results support prior observations by Urquhart *et al.* (2007) that ATCNGC11, 12 and ATCNGC11/12 are localized to the plasma membrane in yeast. Taken together, we concluded that the localization of ATCNGC11/12:E519K is not different from that of ATCNGC11/12, indicating that the E519K mutation in ATCNGC11/12 does not disrupt proper subcellular localization.

3.7 E519 is essential for the channel function not only for ATCNGC11/12, but also for the wildtype channel ATCNGC12

To investigate if the E519K mutation abolishes ATCNGC11/12 channel function, complementation analysis using a yeast mutant, CY162 (Gaber *et al.,* 1988; Ko and Gaber, 1991) lacking its two major K^+ channels, *trk1, trk2* was performed. It has been reported that ATCNGC11, 12 and ATCNGC11/12 are capable of acting as cAMP activated K^+ channels in this K^+-uptake deficient yeast mutant (Yoshioka *et al.*, 2006). As shown in Figure 16a, the mutant yeast carrying *ATCNGC11/12:E519K* does not grow on media in the presence of low K^+, whereas the yeast expressing either *ATCNGC12* or

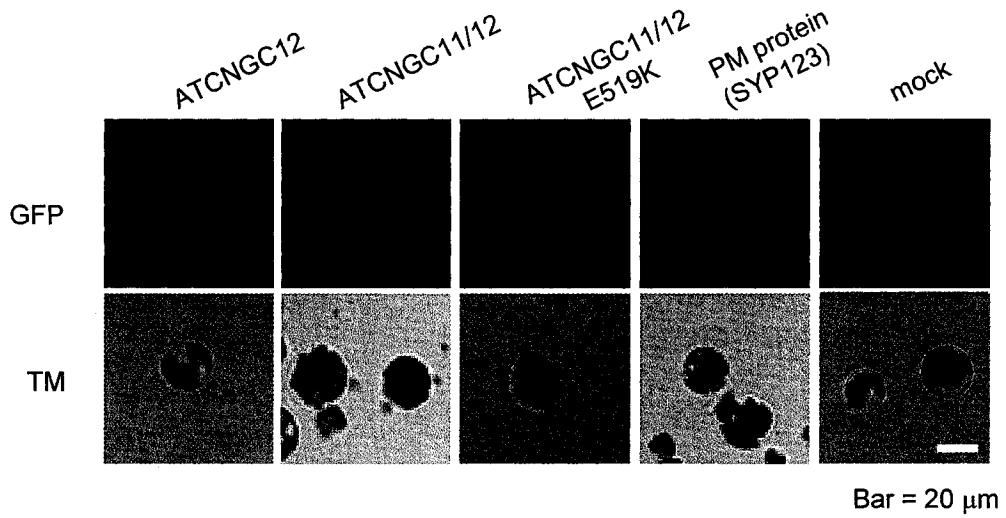

Figure 15. Subcellular localization is not affected by the E519K mutation in ATCNGC11/12. Top panel (GFP): Localization of ATCNGC12, ATCNGC11/12 and ATCNGC11/12:E519K was observed in *Arabidopsis* protoplasts transfected with the plasmid (pMB3) carrying the cDNA for each channel with the smGFP-fusion tag at the C-terminus. A plasma membrane protein (SYP123; Uemura et al., 2004) and untransfected protoplasts were used as positive and negative controls for GFP visualization, respectively. Bottom panel (TM): Protoplasts were observed under transmission light. Images courtesy of Dr. Kato, University of Louisiana.

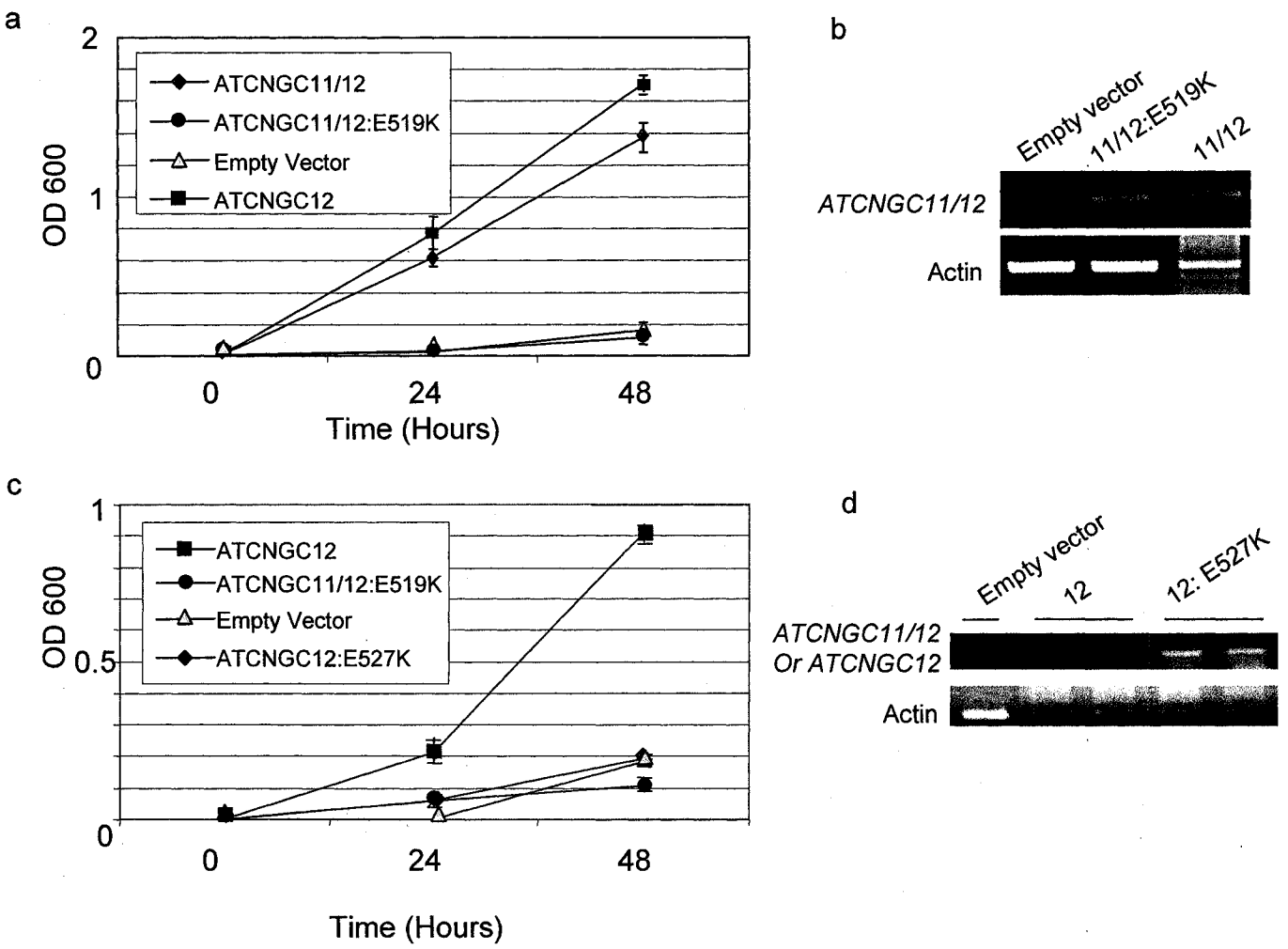

Figure 16. E519/527 is important for channel function in ATCNGC11/12 and ATCNGC12, respectively. (a) *ATCNGC11/12, 12* and *ATCNGC11/12:E519K* were heterologously expressed in the K^+ uptake-deficient yeast strain CY162 and only *ATCNGC11/12* and *12* were able to complement the yeast growth in low K^+ media, whereas *ATCNGC11/12:E519K* has the same minimal growth as the yeast carrying the empty vector (pYES2). (b) Expression analysis of *ATCNGC11/12* in CY162 grown in high K^+ media, carrying the empty vector, *ATCNGC11/12*, or *ATCNGC11/12:E519K* by RT-PCR; see supplementary information for primers used. (c) *ATCNGC12*, *ATCNGC11/12:E519K*, *ATCNGC12:E527K* and the empty vector were heterologously expressed in CY162. Only *ATCNGC12* was able to complement the CY162 growth whereas *ATCNGC12:E527K* has the same minimal growth as *ATCNGC11/12:E519K* and the empty vector. (d) Expression analysis of *ATCNGC11/12* or *ATCNGC12* (because the primers used anneal to the half of *ATCNGC11/12* contributed by *ATCNGC12*) by RT-PCR.

ATCNGC11/12 grow well, indicating that E519K disrupts K^+ channel function of ATCNGC11/12.

Next, we asked if E519 is important for the constitutive active feature of ATCNGC11/12, or for CNGC channel function in general. To address this question, the same point mutation was artificially created by site-direct mutagenesis in the wildtype gene *ATCNGC12* (*ATCNGC12:E527K*). (Note: the residue numbers in ATCNGC11/12 and ATCNGC12 are not the same because the first half of ATCNGC11/12 came from ATCNGC11 gene and it is shorter than that of ATCNGC12. Consequently, E519 in ATCNGC11/12 is E527 in ATCNGC12). As shown in Figure 16c, the yeast carrying *ATCNGC12:E527K* grew similar to the yeast carrying *ATCNGC11/12:E519K* or the empty vector. The expression *ATCNGC12, ATCNGC11/12, ATCNGC11/12:E519K* and *ATCNGC12:E527K* in CY162 was confirmed by RT-PCR and there is no significant difference in the level of gene expression (Figure 16b and 16d). Taken together, these results indicate that E527 is a functionally important residue in the wildtype channel ATCNGC12 and not only to the constitutive activity of ATCNGC11/12.

3.8 E519/527 is well conserved in plant CNGCs and a residue at this position in the CNGA3 of human rod photoreceptors causes total color blindness

Multiple sequence alignment (MSA) of the amino acid sequence of the cytosolic C-terminus from the 20 members in the *Arabidopsis* CNGC family resulted in the same five subgroups (I-IVb) as predicted by a MSA based on the entire gene sequence (Mäser *et al.*, 2001) (Figure 17). ATCNGC12 falls into subgroup I, yet it is remarkably different from the members of this group. Since the C-terminus region contains regulatory domains, this suggests that the regulation of the ATCNGC12 subunit may be different

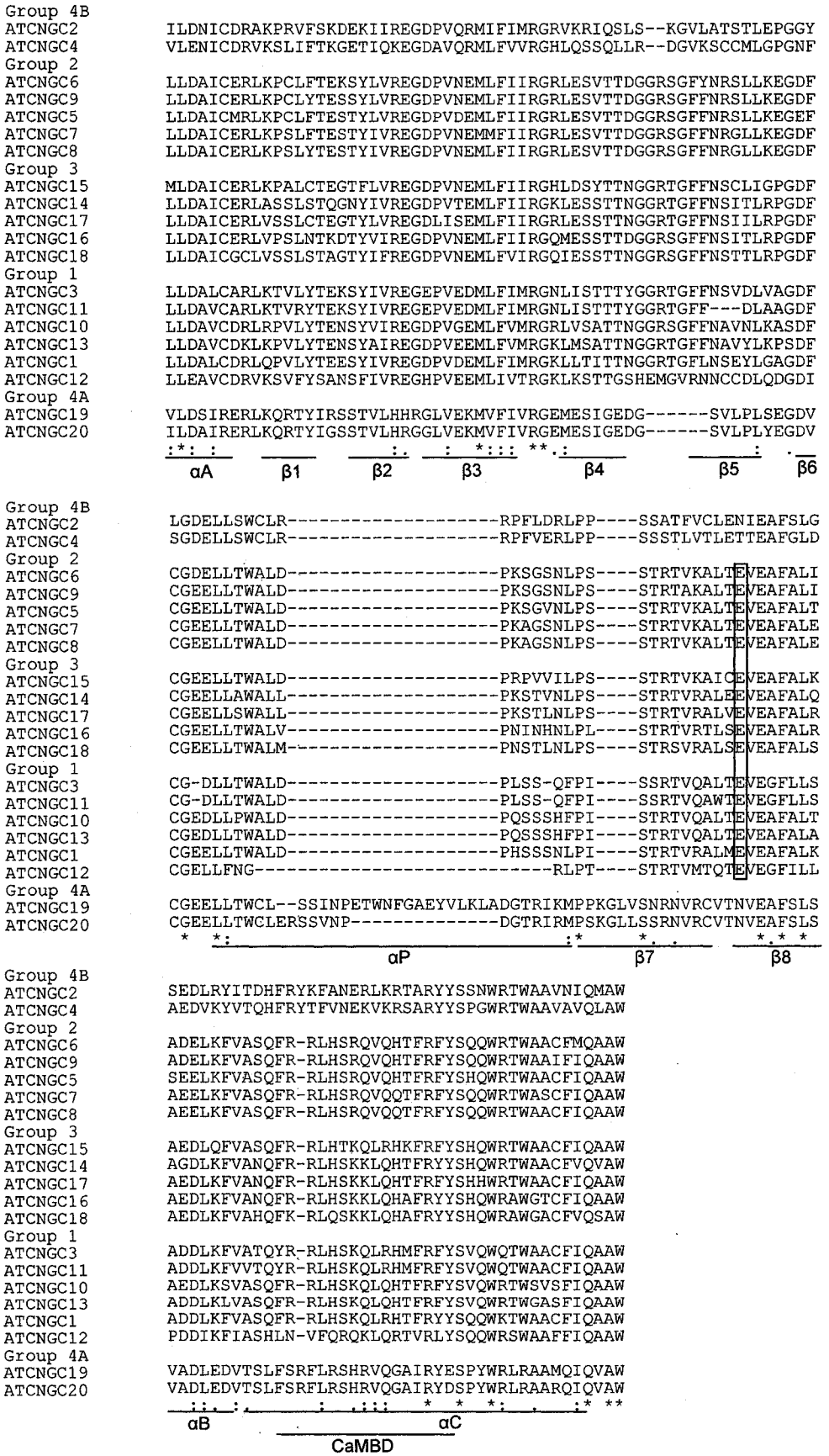

Figure 17. A MSA of the CNBD protein sequences from the 20 members of the *Arabidopsis* (Col-0 ecotype) CNGC family. Using ClustalW, the sequences were aligned into the 5 subgroups determined by Mäser *et al.* (2001). E527 is conserved in 16 of the ATCNGCs; highlighted in red box.

from that of the others (Mäser *et al.*, 2001). Despite this, the E519/527 residue is still well conserved in 16 of the 20 members (Figure 17). Furthermore, this conservation is also observed in known CNGCs of other plant species such as rice, tobacco, bean, and barley, indicating the importance of this residue for their function (Figure 18a). The MSA in Figure 17 predicts residue E519/527 resides at the beginning of the 8^{th} β-strand.

Our alignment of the CNBD sequences with that of the mammalian CNGCs (CNGA1-4 and CNGB1 and 3) and HCN channels (HCN1-4) reveals a highly conserved tyrosine (Y) at the E519/527 position (Figure 18b). Considering that plant and animal maintain a similar structure of CNGCs, this finding suggests that the position of E519/527 is important for channel structure universally. Furthermore, it has been reported that a mutation at this tyrosine in CNGA3 of rod channels causes complete color blindness in humans (Wissinger *et al.*, 2001), supporting this idea. To investigate this idea further, we have conducted a comparison of ATCNGC12 and HCN2 using computational modeling with PYMOL (http://www.pymol.org). As shown in Figure 19, the position E527 perfectly superimposed to this tyrosine residue. This indicates that the position of the glutamate in E527 is structurally important for CNGC channel function in both plant and animals.

3.9 The E519K mutation does not affect cAMP binding: Computational modeling suggest the importance of E519/527 for stabilization of inter-subunit interactions

Crystallization of the CNBD portion from the catabolite activator protein (CAP), the RIα (protein kinase A subunit) and the hyperpolarization-activated cyclic nucleotide-gated (HCN2) has determined that the CNBD interacts with the cyclic nucleotide at the

a

```
Rice (CNGC7)        PTSTRTVMTQTEVEGFILLPDDIKFIASHLNVFQRQKLQRTVRLYSQQWRSWAAFFIQAAW
ATCNGC12            PTSTRTVMTQTEVEGFILLPDDIKFIASHLNVFQRQKLQRTVRLYSQQWRSWAAFFIQAAW
Barley (CNGC1)      PTSTRTVMTQTEVEGFILLPDDIKFIASHLNVFQRQKLQRTVRLYSQQWRSWAAFFIQAAW
Bean (CNGC-C)       PTSTRTVQTLSEVEAFALKADDLKFVASQFRRLHSKQLRHTFRFYSQQWRSWAACFIQAAW
Tobacco (CBP4)      PISTRTAQALSEVEAFALVADDLKLVASQFRRLHSKQLRHTFRFYSGQWRTWAACFIQAAW
```

b

```
CNGA1 (human)           VTQFVVLSDGSYFGEISILNIKGSKAGNRRTANIKSIGYSDLFCLSKDDLMEALTEYPDA
CNGA3 (human)           VTQFVVLSDGSYFGEISILNIKGSKSGNRRTANIRSIGYSDLFCLSKDDLMEALTEYPEA
ATCNGC11/12:E519K       EMGVRNNCCDLQDGDICGELLFNGSRLPTSTRTVMTQTKVEGFILLPDDIKFIASHLNVF
ATCNGC12                EMGVRNNCCDLQDGDICGELLFNGSRLPTSTRTVMTLTEVEGFILLPDDIKFIASHLNVF
HCN2 (human)            KE--MKLSDGSYFGEICLLTR------GRRTASVRADTYCRLYSLSVDNFNEVLEEYPMM
```

Figure 18. E527 is conserved in plant CNGCs and aligns to a tyrosine necessary for colour vision in an animal rod CNGC. (a) ATCNGC12 was aligned to the protein sequence of the CNBDs from putative CNGCs in rice (*Oryza sativa* ,gi 77555620), barley (*Hordeum vulgare* ,gi 66933082), bean (*Phaseolus vulgaris* ,gi 24943196) and tobacco (*Nicotiana tabacum* ,gi 6969231). (b) MSA alignment of the mammalian rod channels CNGA1 (*Homo sapiens,* GI:71143141) and CNGA3 (*Homo sapiens,* GI:4502917) and another mammalian CNBD ion channel, HCN2 *(Homo sapiens*, GI:156071470), were aligned to ATCNGC12 and ATCNGC11/12:E519K which identifies a conserved tyrosine among mammalian channels at this residue location.

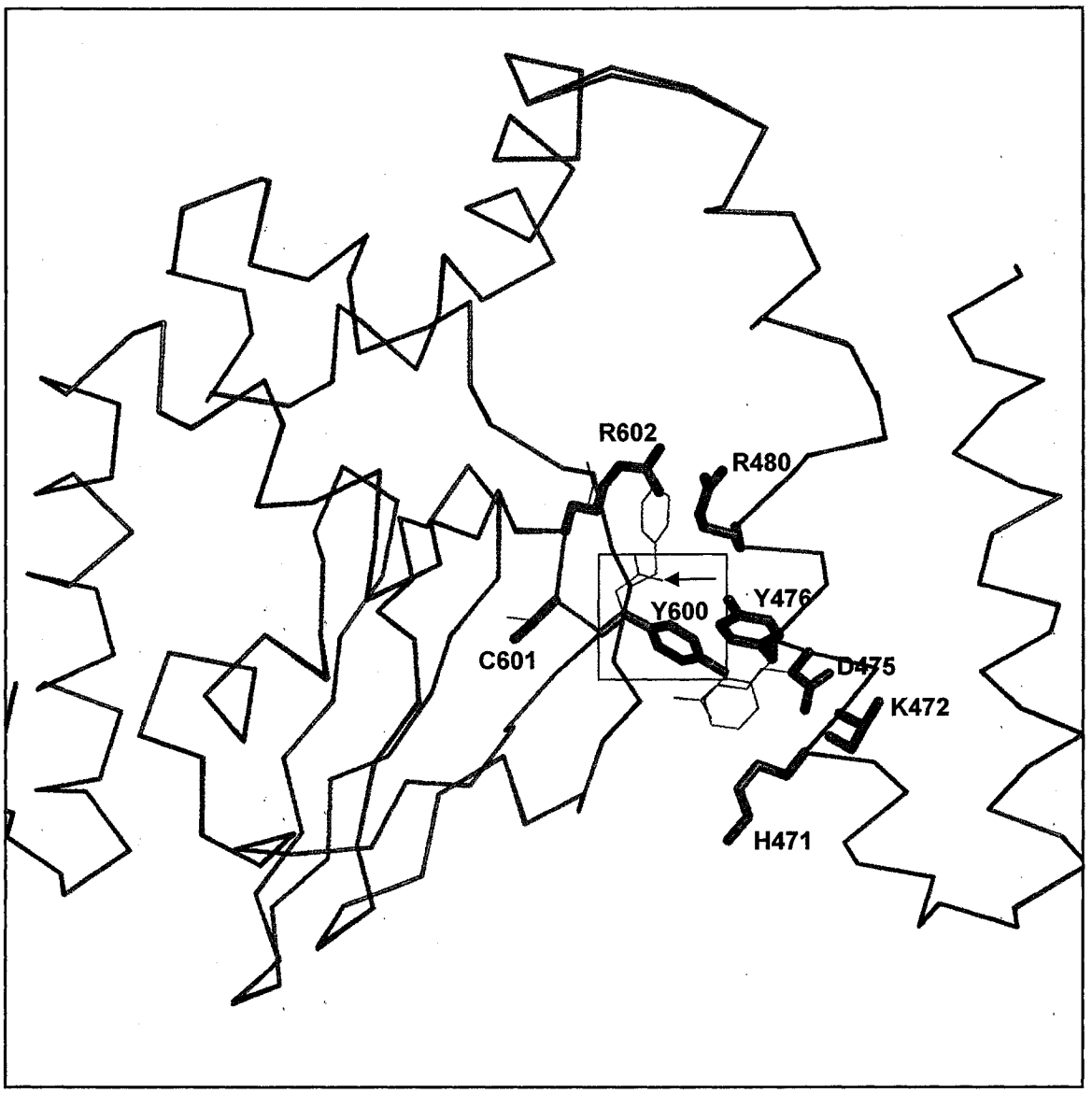

Figure 19. ATCNGC12 CNBD protein sequence superimposed to the crystallized HCN2 (PDB#1Q50) structure. ATCNGC12 (green) residues are shadowed in the background of HCN2 (blue) residues. Y600 in HCN2 aligns to E527 (pointed out in the background with an arrow).

purine ring and the ribofuranose moiety (Berman *et al.*, 2005). The crystallized structure of RIα was modeled to ATCNGC2 and from this analysis three residues in ATCNGC2 that interact with cAMP were predicted (Hua *et al.*, 2003b). A MSA of the CNBD protein sequence from plant CNGCs revealed that the E519/527 does not align with any residues predicted to interact with the cyclic nucleotide in ATCNGC2. This suggests that E519/527 does not interrupt the binding with cyclic nucleotide directly.

To confirm that cyclic nucleotides would still bind to the CNBD with the E519/527K mutation, the CNBD portion of ATCNGC12 (CNBD12) and ATCNGC11/12:E519K (CNBD11/12:E519K) was expressed in *E. coli* BL21 cells. Soluble proteins were then extracted and purified using a Ni^{2+}-affinity column. These purified proteins were tested for binding capabilities to cAMP using cAMP-agarose (Sigma-Aldrich). The amount of protein which binds to the cAMP resin was almost equal for both CNBD12 and CNBD11/12:E519K (Figure 20a), suggesting that the E519 mutation does not disrupt the CNBDs ability to bind to cAMP. The negative control (aconitase, Moeder *et al.*, 2007) shows no significant binding to the resin under the same condition (Figure 20b).

cAMP was tested for the binding assay first, since previous work had shown that ATCNGC11, 12 and ATCNGC11/12 are activated by cAMP but not cGMP in a yeast complementation assay (Yoshioka *et al.*, 2006). However, since this experiment was conducted in yeast, the possibility that cGMP binds to ATCNGC12 or that the E519K mutation causes an alteration in ligand specificity can not be ruled out. To address these points, we asked if cGMP binds to ATCNGC11/12 or ATCNGC11/12:E519K. To test this, we conducted a competition analysis using cGMP and cAMP. Both expressed

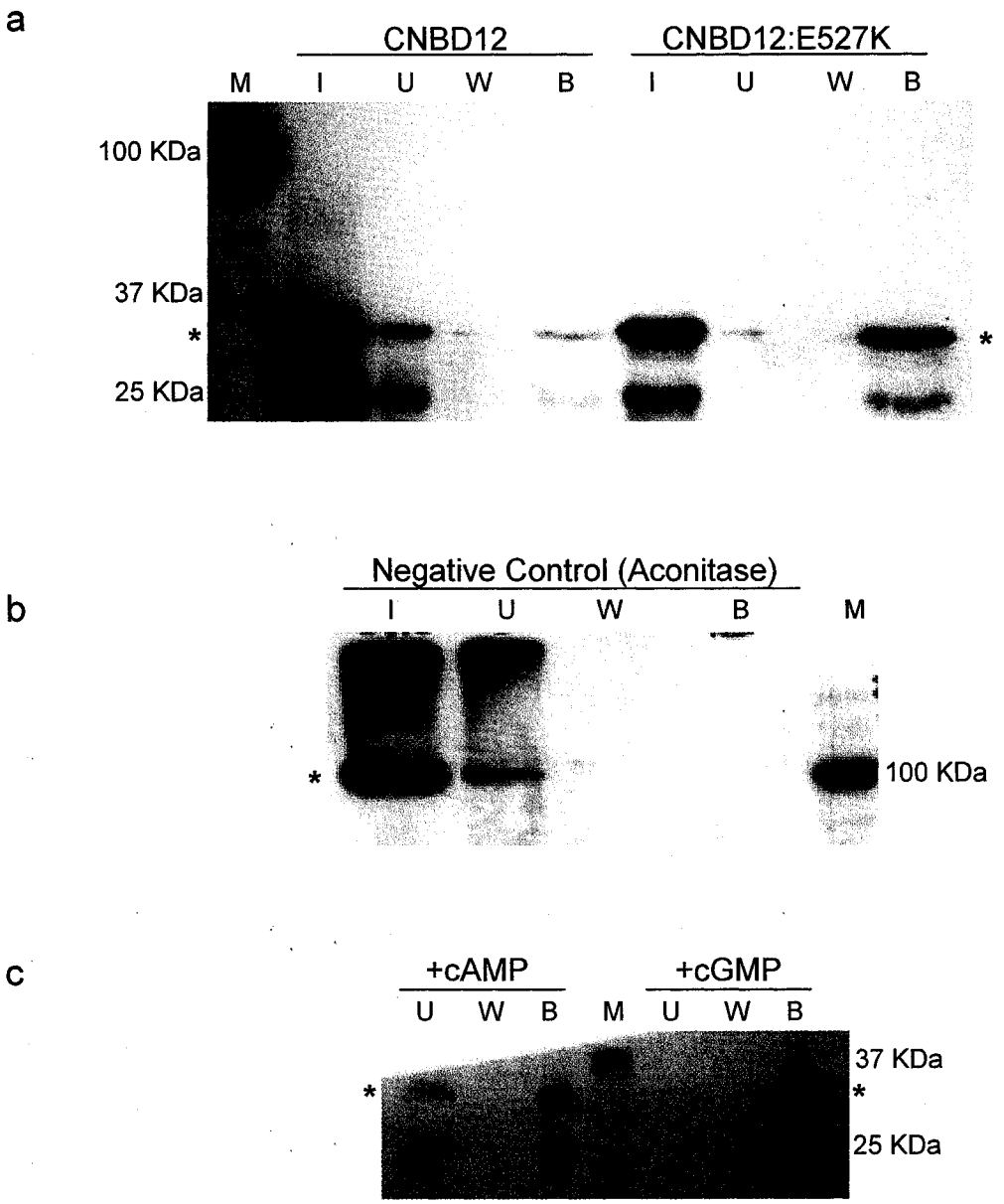

Figure 20. cAMP binding assay under high stringency conditions (500 mM NaCl) to demonstrate specific interactions with the ligand. Western blot analysis with a His-tag antibody to detect the His-tag present in all of the purified proteins. Legend: marker (M), input (I), unbound (U), first wash (W), protein bound to cAMP resin (B). (a) CNBD proteins for ATCNGC12 and ATCNGC12:E527K. (b) Control protein, aconitase, does not interact with cAMP resin. (c) Competition assay with CNBD12 incubated with either cAMP or cGMP prior to adding the cAMP resin. An (*) indicates the expected protein size. The lower band is likely a product of protein degradation.

proteins were pre-incubated with either cAMP or cGMP and then cAMP agarose was added. As shown in Figure 20c, prior incubation of CNBD12 with cAMP competed well and reduced binding to the cAMP resin, whereas incubation with cGMP did not affect binding to cAMP agarose (Figure 20c), indicating that cGMP does not bind to CNBD12. These results are consistent with previous observations (Yoshioka *et al.*, 2006), indicating that there is specific binding of cAMP over cGMP for activation of ATCNGC12. However, the result of CNBD11/12:E519K interacting with cAMP specifically over cGMP is inconclusive at this time due to lack of protein expression. Therefore, further analysis is required.

Since E519 is not predicted to interact with cAMP and the cAMP binding assay shows that the CNBD11/12:E519K can still bind to cAMP, the role E519 has in ATCNGC11/12 was further investigated. First, the entire cytosolic C-terminus of ATCNGC12 was modeled based on the crystallized structures of RIα. As shown in Figure 21, it appears that the side chain of the glutamate at E527 faces away from the interior of the pocket formed by the β-barrel that is thought to accommodate the binding of a cyclic nucleotide, supporting our observation that E527 does not interfere the cyclic nucleotide binding. Also, modeling the C-terminus of ATCNGC12 and ATCNGC11/12:E519K, using the crystallized structure of HCN2, predicted the same interactions as when modeled to RIα. According to this modeling, E519/527 interacts with residues on the B-helix of the C-linker (Figure 22a and b).

As shown in the super-imposition of the predicted CNBD structure of ATCNGC11/12 and ATCNGC11/12:E519K (Figure 22c), there is a change in the predicted interaction between E519K and other surrounding residues. This alteration of

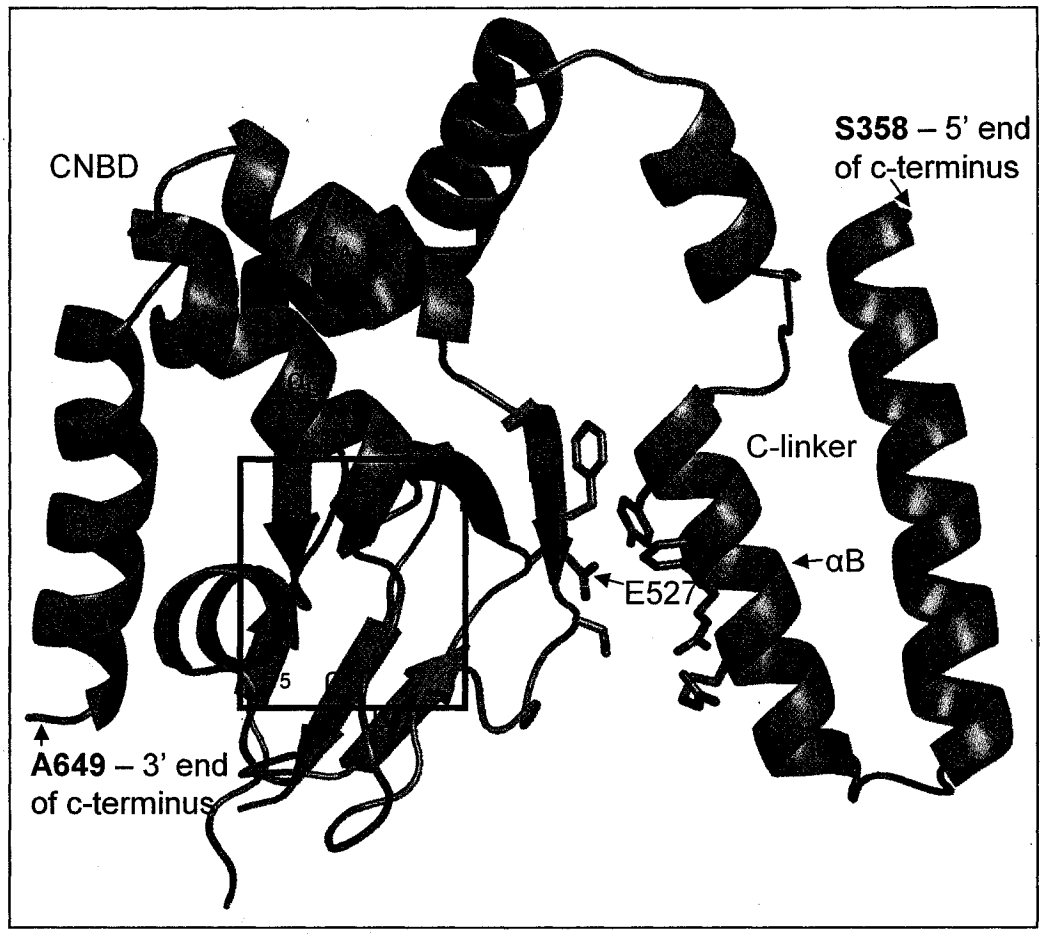

Figure 21. Predicted ATCNGC12 C-terminus tertiary protein structure. The protein sequence from the residues after the sixth transmembrane domain (S358 to A649) of ATCNGC12 were modelled to the crystallized RIα (PDB#1NE6), and predicted the eight beta strands (β1-β8) and the three alpha helices (αA-αC) of the CNBD and the C-linker. A pocket is created by the β-barrel which is were a cAMP (red circle) would reside. The E527 residue faces away from the cAMP and towards the B-helix (αB) in the c-linker.

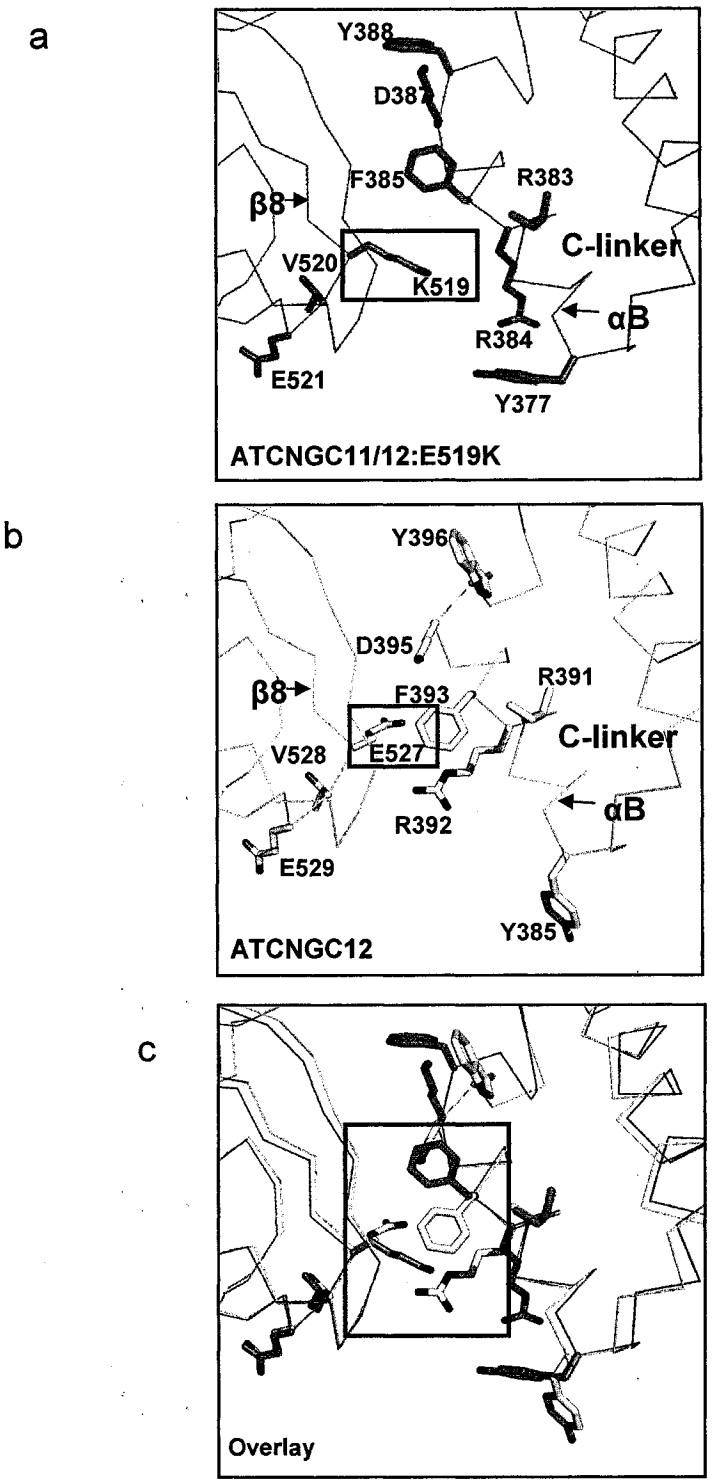

Figure 22. Predicted tertiary structure of the CNBD of ATCNGC11/12 (or ATCNGC12) with and without the E519K mutation. Both ATCNGC11/12:E519K and ATCNGC12 were modeled to the crystallized HCN2 (PDB#1Q50) using PYMOL. (a) predicted protein interaction of E519K on the eight beta-strand (β8) with neighbouring residues from the B-helix (β8) in the C-linker. R384 is shown to be within the closest proximity for protein interaction. (b) predicted protein interaction with E527 remains the arganine (R392 is R384 in ATCNGC12). (c) ATCNGC12 and ATCNGC11/12:E519K superimposed, predicts how a lysine replacing E519/527 would change the position of surrounding amino acids and appears to push away R384/392.

protein interactions is hypothesized to destabilize both intra- and inter-subunit interactions between the C-linker. The negative charge of E519 could be forming strong salt bridges between positively charged R384. Replacing the glutamate with a positively charged lysine (E519K) would destroy this salt bridge. Also, the arganine and the lysine are both positively charged which could cause repulsion instead of an interaction. The loss of interaction of E519 and R384 also appears to affect neighbouring interactions between the B-helix of the C-linker and the CNBD (Figure 22c). Take together, we conclude that the E519K mutation does not affect cyclic nucleotide binding; rather it may interfere with the stabilization of inter-subunit interactions.

CHAPTER 4 – Discussion

4.1 Suppressor screening of *cpr22*

In the suppressor screen for the *cpr22* mutant a variety of morphological phenotypes were observed. Based on morphological phenotypes, they were categorized into six groups. The morphological phenotype of group I plants is similar to that of wildtype plants. Suppressor #73 is a member of group I and sequencing revealed a point mutation in *ATCNGC11/12* which caused a residue change from a glutamate to a lysine (E519K). We originally hypothesized that the suppressors with a wildtype phenotype would be good candidates to identify downstream components in the *cpr22*-mediated pathogen resistance pathway because the strong morphological difference from *cpr22* could be beneficial for subsequent map based cloning. Instead, we have shown that the suppressors with intragenic mutations in *ATCNGC11/12*, like suppressor #73, can be used to identify important residues for the function of the channel.

A similar situation was reported in the suppressor screening of the *acd6-1* mutant. a*cd6-1* (Accelerated Cell Death *6*) is a lesion mimic mutant which has a gain of function mutation in the *ACD6* gene (Rate *et al.*, 1999). *ACD6*, encodes a novel protein containing ankyrin repeats and putative transmembrane (TM) regions (Lu *et al.*, 2003). *acd6-1* has a single amino acid change in the TM of ACD6. A screen to identify suppressors for *acd6-1* was conducted using EMS and the suppressor candidates were categorized into two groups, one of which were identical to wildtype and the other were wildtype with HR-like lesions (Lu *et al.*, 2005). It was found that all seventeen suppressors of *acd6-1* with a wildtype phenotype had intragenic point mutations which caused residues changes at positions important for the function of *ACD6*.

In our screen, so far 45 suppressors with a wildtype phenotype were found to be intragenic mutants, similarly to the *acd6-1* suppressors. The location of majority of the intragenic mutations in were found in the cytosolic C-terminus, throughout the C-linker and the CNBD. The large number of intragenic mutations indicates the difficulty of suppressor screens for gain of function mutants. Yoshioka *et al.*, (2001) showed that salicylic acid (SA) accumulation is responsible for the *cpr22* phenotype. Therefore, if this suppressor screening was saturated, then SA biosynthesis genes, like *SID2* (Wildermuth *et al.*, 2002), should have been identified. However, so far we have not identified a suppressor with a mutation in *SID2*. Therefore, our and the *acd6* suppressor mutant screening were also likely not saturated. Further screening may be required in order to find downstream components.

4.2 The E519K mutation in *ATCNGC11/12* suppresses *cpr22*-related phenotypes yet does not effect channel subcellular localization

The enhanced disease resistance in *cpr22* involves constitutive expression of defense-related genes, such as *PR-1*, and the induction of a HR-like cell death. Suppressor #73 lost constitutive expression of *PR-1* and lesion formation, suggesting that the E519K mutation identified in the CNBD of *ATCNGC11/12* was responsible for suppression of these phenotypes. Recently, we have reported that the transient expression of *ATCNGC11/12* by *Agrobacterium* infiltration causes HR-like programmed cell death in a Ca^{2+} dependent manner (Urquhart *et al.*, 2007). This method is very useful to observe cell death since development of cell death is well synchronized. Therefore, in this study we used this system to evaluate *ATCNGC11/12:E519K* in *N. benthamiana*. As we expected, the E519K mutation caused no lesion formation, unlike the expression of

ATCNGC11/12. The loss of HR-like lesion formation on *N. benthamiana* leaves after infiltration with *Agrobacterium* carrying *ATCNGC11/12:E519K* supported the hypothesis that this mutation is responsible for suppressing the *cpr22*-related phenotypes by abolishing ATCNGC11/12 activity.

The loss of *cpr22*-related phenotypes was assumed to be due to the alteration of ATCNGC11/12 at the protein level since the gene expression levels of *ATCNGC11/12* (with mutation E519K) in suppressor #73 were comparable to that of *cpr22* plants. This led us to investigate the subcellular localization of ATCNGC11/12. Previously some studies have shown how single point mutations in the CNBD of an ion channel can prevent protein localization. Improper protein localization in the ion channel HERG was first reported by Zhou *et al.* (1998), which was caused by a mutation in the seventh β-strand of the CNBD. These results were further investigated by Ficker *et al.* (2002) and Akhavan *et al.* (2005). They provided evidence that a mutation in the seventh β-strand or one in the sixth β-strand inhibit proper localization of HERG ion channels. Other reports of improper protein localization for HERG ion channel were reported for mutations created in the A- and C-helices (Satler *et al.*, 1996; Ficker *et al.*, 2000; Akhaven *et al.*, 2003). The CNBD B- and C-helices in their entirety have also been reported as necessary for localization of HCN2 channels (Proenza *et al.*, 2002b; Akhaven *et al.*, 2005). These are key areas in the CNBD that directly interact with the ligand. E519 does not align to any of the residues found in HCN2 which prevented proper localization when mutated.

Recently, ATCNGC11/12, ATCNGC11 and 12 where shown to localize to the plasma membrane of yeast cells (Urquhart *et al.*, 2007). In this study, to observe the localization to the plasma membrane *in planta*, many attempts were made using tobacco

BY-2 cells, transgenic *Arabidopsis* lines and protoplast transfection. Yet all attempts were inconclusive. After collaborating with Dr. Kato at the University of Louisiana the localization of ATCNGC11/12:E519K-smGFP fusion protein was observed in the plasma membrane of *Arabidopsis* protoplast cells. This confirms that the E519K mutation does not affect proper subcellular localization of ATCNGC11/12.

The reason why we could not succeed to observe the subcellular localization is not known. It could be due to the lack of our expertise or a fundamental technical problem. However, one piece of information that is worth mentioning is that, although Dr. Kato's laboratory succeeded to obtain the localization images, the rate of transfection was very low. According to their record, the transfection rate was approximately 3%. Compared to the other protein transfections in their laboratory, which routinely show approximately 25%, a 3% success rate is remarkably low. This could be due to a high turnover of the CNGCs in the transfected cells or poor expression of the CNGCs in the vector. Further investigation is necessary to find the reason of this low transfection rate.

4.3 E519 is essential for CNGC channel function

Plant CNGCs differ from animal CNGCs in that they can discriminate against certain ions. To determine ion selectivity of plant CNGCs, heterologous expression analyses in *Saccharomyces cerevisiae* mutants deficient in cation uptake have been used. One such yeast mutant, CY162, lacking two major K^+-uptake transporters, *trk1, trk2*, (Gaber *et al.,* 1988; Ko and Gaber, 1991) has been used in this study. This strain is similar to the yeast strain WD3 which has been used to examine ATCNGC11, and 12 and ATCNGC11/12 channel function (Yoshioka *et al.*, 2006). The CY162 strain has

previoysly been used to examine ATCNGC10 and 2 and the CNGC from barley, HvCBT1 (Schuurink *et al.*, 1998; Leng *et al.,* 1999; Li *et al.*, 2005). ATCNGC10 and 2 were able to complement the K^+ up-take deficiency at low potassium concentrations but not HvCBT1. However, Leng *et al.*, (1999) found that ATCNGC2 could only complement the CY162 strain with the addition of cAMP. These results were contradicted when a different K^+-uptake deficient yeast strain was used to express *ATCNGC2*, in which ATCNGC2 could complement the mutation even in the absence of cAMP (Köhler *et al.*, 1999; Mercier *et al.*, 2004). Other *Arabidopsis* CNGCs, ATCNGC1, 3 and 4, were also able to complement the K^+-uptake deficient mutation without the presence of cAMP (Mercier *et al.*, 2004; Gobert *et al.*, 2006)

Later, the protocol for the complementation of the K^+ uptake-deficient yeast was modified by Dr. G. Berkowitz's laboratory at the University of Connecticut. Addition of the antibiotic hygromycin B causes hyper-polarization of the plasma membrane and this hyper-polarization can suppress the background growth of the yeast mutant (Madrid *et al.*, 1998; Bihler *et al.*, 2002). ATCNGC1, 2 and 4 were all still able to complement the K^+ up-take deficiency of this yeast mutant with this revised protocol (Mercier *et al.*, 2004). However, yeast growth was enhanced with the addition of membrane-permeable cAMP, indicating the clear activation of the channel by cAMP. Later, the same modified assay was used to evaluate *ATCNGC11, 12* and *ATCNGC11/12*, and all three genes were able to complement the mutant yeast both with and without cAMP, but the addition of cAMP did enhance the complementation efficiency (Yoshioka *et al.*, 2006).

Since ATCNGC11/12 was able to complement the K^+ up-take deficiency, this method was used to asses the effect of the E519K mutation in ATCNGC11/12 on K^+

channel function. As we expected, ATCNGC11/12:E519K was unable to complement the K^+ up-take deficiency of CY162. This result strongly indicates the importance of this residue in ATCNGC11/12 channel function. Furthermore, in this study we showed that E519 is not only necessary for the ATCNGC11/12 function but also for the wildtype channel ATCNGC12. This study combined with the finding of a high conservation of E519/527 in plant CNGCs, suggests that the residue at this location has a structural importance to the tertiary structure of the CNBD in general.

A multiple sequence alignment (MSA) of the CNBDs from ATCNGC11/12 and CNGA3 and the computational modeling of CNBD11/12:E519K to HCN2 revealed that E519 aligns to Y573 in CNGA3 and Y600 in HCN2 (Figure 18). Although the molecular mechanism is not clear yet, a clinical study of the CNGCs in human cone receptors showed that a mutation at this Y573 in CNGA3 caused total colour blindness (complete achromatopsia) (Wissinger *et al.*, 2001). This tyrosine is conserved well in the mammalian ion channels and it has been shown that CNBDs demonstrate a high level of secondary structure conservation (Canaves and Taylor, 2002). Therefore, it is reasonable to conclude that residue at this location is structurally important. Further comparison between CNGA3 human mutants and *cpr22* intragenic mutants may reveal other functionally important positions in the structure of this type of channel. In this scenario, since ATCNGC11/12 is a unique constitutive active channel, it will be a useful tool to reveal important residues for channel function by suppressor screening or site-directed mutagenesis.

4.4 The E519K mutation in *ATCNGC11/12* does not interfere with the binding of cAMP to the CNBD

Activation of CNGC by cyclic nucleotides (cAMP/cGMP) has previously been demonstrated indirectly in mammalian CNGCs electro-physiologically using heterologous expression analysis in *Xenopus laevis* oocytes and human embryonic kidney (HEK) cells (Zagotta and Siegelbaum, 1996). It has been reported that the current level can vary between rod and olfactory CNGCs depending on the type of cyclic nucleotide which binds to the CNBD of the channel, indicating the specificity of ligand-binding in CNGCs (Gordon and Zagotta, 1995b; Varnum *et al.*, 1995; Shapiro and Zagotta, 2000). However, the expression of plant CNGCs in *Xenopus* oocytes and HEK cells has been unsuccessful in patch-camp analyses, most likely due to the instability of plant genes in these heterologous systems (Leng *et al.*, 2002; Hua *et al.*, 2003; Berkowitz, personal communication). Therefore, in this study, a direct binding assay was taken to analyze if this mutation prevents the binding of cyclic nucleotides.

To test the direct binding of ATCNGCs with cyclic nucleotides, a cAMP-bound agarose resin was utilized. Previously, this resin was used to evaluate the ability of mammalian cAMP-binding proteins (cAMP-GEFs) to bind to cAMP (Kawasaki *et al.*, 1998). The analysis of CNBD12 and CNBD11/12:E519K proteins with the cAMP resin concluded that the E519K mutation does not disrupt the binding of cAMP (Figure 21a). Even under high stringency (500 mM NaCl) conditions, the interaction between the CNBDs from ATCNGC12 or ATCNGC11/12:E519K, and cAMP resin was observed. This indicated that the interaction of the CNBDs with the cAMP resin is a strong, stable interaction.

As already mentioned, it has been reported that ion channels with CNBDs have specific cyclic nucleotide agonists. Mammalian CNGCs are activated only by cGMP whereas HCN channels are activated fully by cAMP and only slightly by cGMP (Kaupp and Seifert, 2002). By incubating the CNBD12 and CNBD11/12:E519K proteins with cAMP or cGMP prior to treating the proteins with the cAMP resin, we attempted to demonstrate that these CNBD proteins have specific interactions with one cyclic nucleotide over another. Preliminary results demonstrate that CNBD12 specifically interacts with cAMP but not cGMP. We are currently trying to conclude if CNBD11/12:E519K also specifically interacts with cAMP. This analysis has been attempted several times but the amount of protein appears to be crucial and the expression levels of the CNBDs have been quite low.

These results are the first to show the binding of cAMP to a plant CNGC directly. This assay could prove very useful to identify important residues necessary for interacting with cyclic nucleotides combined with computational modeling analyses. Crystallography is one of the best ways to predict cyclic nucleotide interactions with the residues in the CNBD. However, crystallization of proteins can be very time consuming and does not reveal all functional conformations of the protein. Considering the technical difficulty of patch-clamp analysis with plant CNGCs (Leng *et al.*, 2002; Hua *et al.*, 2003), or crystallography, the direct binding assay used in this work may be useful to study the binding site of cyclic nucleotides to plant CNGCs.

It has been reported that there are three residues predicted to interact with cAMP in ATCNGC2 (Hua *et al.*, 2003*b*), located in the phosphate binding cassette (PBC) which binds to the ribofuranose moiety of cAMP. In the CAP CNBD there are four residues in

the PBC which bind to the ribofuranose of cAMP (Punta *et al.*, 2003). Residues which bind to the purine ring of cyclic nucleotides in rod and olfactory CNGCs reside in the fifth β-strand and the C-helix (Scott *et al.*, 2000). As previously mentioned, the purine ring of cyclic nucleotides appears to be involved with ligand selectivity and the ribofuranose moiety is probably required for ligand stabilization. E519/527 does not reside in any of these areas in the CNBD. Therefore, together with our cAMP binding assay, we concluded that the mutation at this residue would not disrupt ligand binding or selectivity.

4.5 The E519K mutation may disrupt the gating of ATCNGC11/12

The cyclic nucleotide binding assay supported the theory that the E519K mutation in ATCNGC11/12 does not disrupt the binding of cyclic nucleotides. Computational modeling was used to further support this theory and predict a possible role of E519 in channel activation and the molecular mechanism of disruption to channel function by this mutation. The computational model of ATCNGC11/12:E519K, which was created based on the crystal structure of HCN2 predicted that E519 interacts primarily with the R384 residue located in the B-helix of the C-linker (Figure 20). Craven and Zagotta (2004) identified a glutamate in the 2^{nd} β-strand of the CNBD of HCN2 and CNGA1 which has a strong interaction with an arginine in the B-helix of the C-linker forming a intrasubunit salt bridge. This salt bridge proved necessary for proper gating in the HCN2 channels. In CNGA1, this intrasubunit salt bridge affected channel activation by altering ligand specificity (Craven and Zagotta, 2004). Even though E519 is not at exactly the same position as the glutamate identified in the HCN2 and CNGA1 channels, the study

demonstrates how the loss of one interaction between two subunits can alter channel function. The E519K mutation would disrupt the potential salt bridge formed with R384.

The inter- and intra-subunit salt bridges formed between residues in the CNBD and the C-linker of HCN2 and CNGA1 channels supports the theory that the E519K mutation could alter channel gating in ATCNGC11/12. Although, unless ATCNGC11/12:E519K is crystallized, it is not possible to determine if E519 is interacting with R384 of its own subunit or that of a neighboring subunit. Six α-helices make up the C-linker in HCN2 (αA- αF) and the first two helices (αA and αB) form an antiparallel helix-turn-helix motif that interacts with the αC and αD helices of the neighbouring subunit (Zagotta *et al.*, 2003; Craven and Zagotta, 2004). This interaction has been explained as an "elbow on shoulder" (Zagotta *et al.*, 2003), and appears to create a partial hydrophobic environment for the interacting amino acids. The A- and B-helix of the C-linker are referred to as the "elbow" that is resting on the C- and D-helix, which is the "shoulder", of a neighbouring subunit (Craven and Zagotta, 2004). This type of interaction between subunits makes it difficult to predict what type of structural change takes place in the C-linker when the E519K mutation is present in ATCNGC11/12. Therefore, we speculate that the E519K mutation has rendered the C-linker in a closed state possibly by disrupting the "elbow on shourlder" interactions. Even with a cyclic nucleotide bound to the CNBD of ATCNGC11/12:E519K, this closed state renders the ATCNGC11/12 channel inactive.

4.6 Future Direction

As we mentioned above, our computational analysis predicted a potential interaction between E519 and R384. This indicates that the disruption of channel function may be due to the disruption of this interaction. To further address this hypothesis, the *N. benthamiana* heterologous expression system can be used. Currently in our laboratory, ATCNGC11/12:R384I was created to see if this mutation causes the same suppression of HR in *N. benthamiana*. A preliminary trial revealed that no lesions formed when *ATCNGC11/12:R384I* was transiently expressed in *N. benthamiana*. This result supports our hypothesis for the necessary interaction of E519 and R384 in ATCNGC11/12. Additionally, it should be tested if the E519K mutation affects on intra-subunit interactions. Although currently we do not know if ATCNGC12 (ATCNGC11/12) forms heterotetramers or homotetramers *in planta*, heterologous expression analysis in yeast indicates that they can form functional homoheteromer K^+ channel *in yeast*. Therefore, we are going to test if subunit interaction (homoheteromer) is disrupted by the E519K mutation. Currently, yeast two hybrid systems using only the C-terminal cytosolic portion of CNGCs are being tested. Furthermore, FRET and split YFP systems also are being tested by a collaborator. Alternatively, co-immunoprecipitation also could be used for a subunit interaction assay.

Other aspects of the ATCNGC11/12:E519K channel function, also have to be addressed. Urquhart *et al.* (2007) showed that Ca^{2+} is important to induce the HR in *N. benthamiana*. Since ATCNGC11/12 and its wildtype channels conduct Ca^{2+} in yeast, we therefore have to test if ATCNGC11/12:E519K can still conduct Ca^{2+}. If

ATCNGC11/12:E519K is unable to conduct Ca^{2+}, this would further support the role the E519K mutation has on channel function.

Also, the competition analysis of cyclic nucleotides has to be repeated and concluded to fully understand the nature of the E519K mutation in ATCNGC11/12. All of these future analyses and the continuous investigation of the other intragenic mutations in ATCNGC11/12 (identified from the rest of the suppressors) will assist to unravel the molecular mechanism of the novel function of the chimeric channel, ATCNGC11/12 and at the same time, identify functionally important residues for wildtype channels.

CHAPTER 5 - Conclusion

The work shown in this thesis revealed that the residue E519 is functionally important for ATCNGC11/12. Also, the position E519 is likely important for the function of the wildtype channel, ATCNGC12, Computational modeling and bioninformatics analyses revealed that the location of this glutamate is important for the structure of the CNBD of one subunit and possibly for the interaction with partner subunits. Finally, the cyclic nucleotide binding assay suggested that this channel likely binds to cAMP and that the E519K mutation does not affect this binding. This project has demonstrated that ATCNGC11/12 is unique and a useful tool to identify functionally important amino acids in CNGCs in general.

APPENDIX-APPENDIX A

Table 1. Primer sequences and melting temperatures (T_m).

Primer	Oligonucleotide sequence	T_m (°C)
cpr22#73_for	5'-CCGTAATGACTCAGACTAAAGTTGAAG GTTTCATTCTCTTGCC-3'	71
cpr22#73_rev	5'-GGCAAGAGAATGAAACCTTCAACTTTA GTCTGAGTCATTACGG-3'	71
D2DT-for	5'-CTCTTGATCCCACTTCC-3'	51
D2DT_rev	5'-GACCGTGAGATTGCAGT-3'	51
#1	5'-ATGGAAAATTGAAAAGTGTTAGAGGA-3'	56
#32	5'-ACGTTTCCAATGAGCACAGCA-3'	57
#10 (for)	5'-TTATACTCACAGCAATGGCG-3'	54
#46 (rev)	5'-CTATGCTTCAGCCTTTGC-3'	52
#67	5'-GGGATCCCATGAATCTTCAGAGGAGAAA-3'	64
#68	5'-CTATGCTTCAGCCTTTGCAAACTC-3'	60
pYES2_fwd	5'-AAGCCGCCGAGCGGGTGACA-3'	64
pYES2_rev	5'-GCTAGTCAGTCCGATCCGGGG-3'	65
ACT1_fwd	5'-CCTACGTTGGTGATGAAGCT-3'	55
ACT1_rev	5'-GTCAGTCAAATCTCTACCGG-3'	55
β-tubulin_fwd	5'-CGTGGATCACAGCAATACAGAGCC-3'	71
β-tubulin_rev	5'-CCTCCTGCACTTCCACTTCGTCTTC-3'	72
Ws14-EcoRI (for)	5'-AAGAATTCGGTTGGCTACTAGAAGCTGTG TCCG-3'	61
#37 (rev)	5'-CACTATGCTTCAGCCTTTGC-3'	63

Table 2. Media and antibiotic selection for bacterial growth.

Bacteria	Plasmid	Medium	Antibiotic Selection
E. coli (DH5α)	pMBP3, pET28a	LB	Kanamycin sulfate (50 µg/ml)
E. coli (DH5α)	pGEM-T Easy, pBluescript, pYES2	LB	Ampicillin (50 µg/ml)
E. coli (BL21)	pET28a	LB	Kanamycin sulfate (50 µg/ml)
Agrobacterium	pMBP3	LB and LB+MES	Kanamycin sulfate (50 µg/ml) and rifampicin (100 µg/ml)

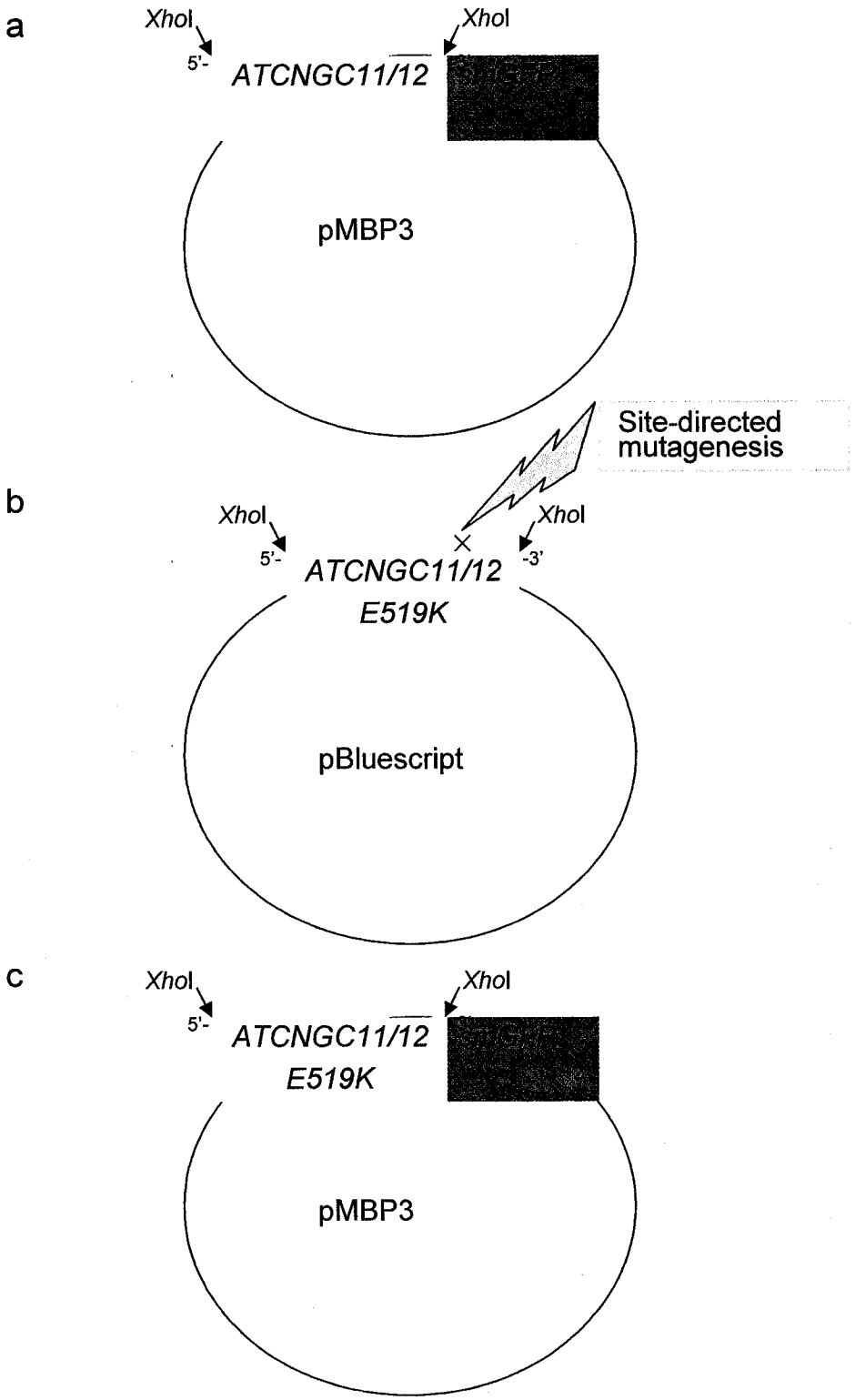

Figure 1. Construction of pMBP3-*ATCNGC11/12:E519K*. (a) pMBP3-*ATCNGC11/12* was digested with *Xho*I to excise *ATCNGC11/12* cDNA, from the vector and without the *smGFP* tag. (b) *ATCNGC11/12* cDNA with *Xho*I cut sites at both 5' and 3'-ends was ligated into pBluescript, linearized with *Xho*I. Site-directed mutagenesis was used to create *ATCNGC11/12:E519K* in pBluescript. (c) *ATCNGC11/12:E519K* cDNA was subsequently digested from pBluescript by *Xho*I and re-ligated back into pMBP3, with the *smGFP* tag is at the 3'-end.

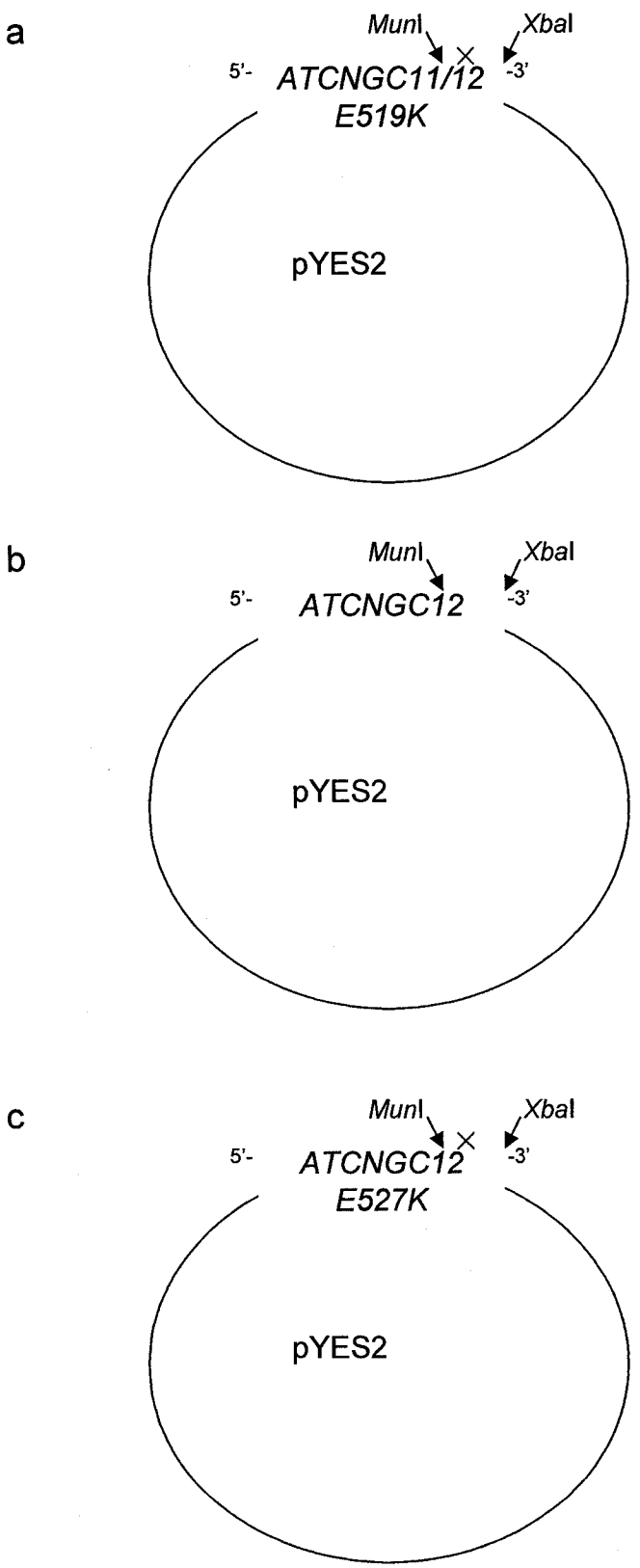

Figure 2. Construction of pYES2-*ATCNGC12:E527K*. The cDNA (a) *ATCNGC11/12:E519K* and (b) *ATCNGC12* in pYES2, have restriction enzyme sites *Mun*I and *Xba*I before and after the E519K mutation (represented by a red 'x'), respectively. Digesting both of these plasmids, (a) and (b), with *Mun*I and *Xba*I, and then subsequently swaping the areas with the mutation created (c) *ATCNGC12:E527K* in pYES2.

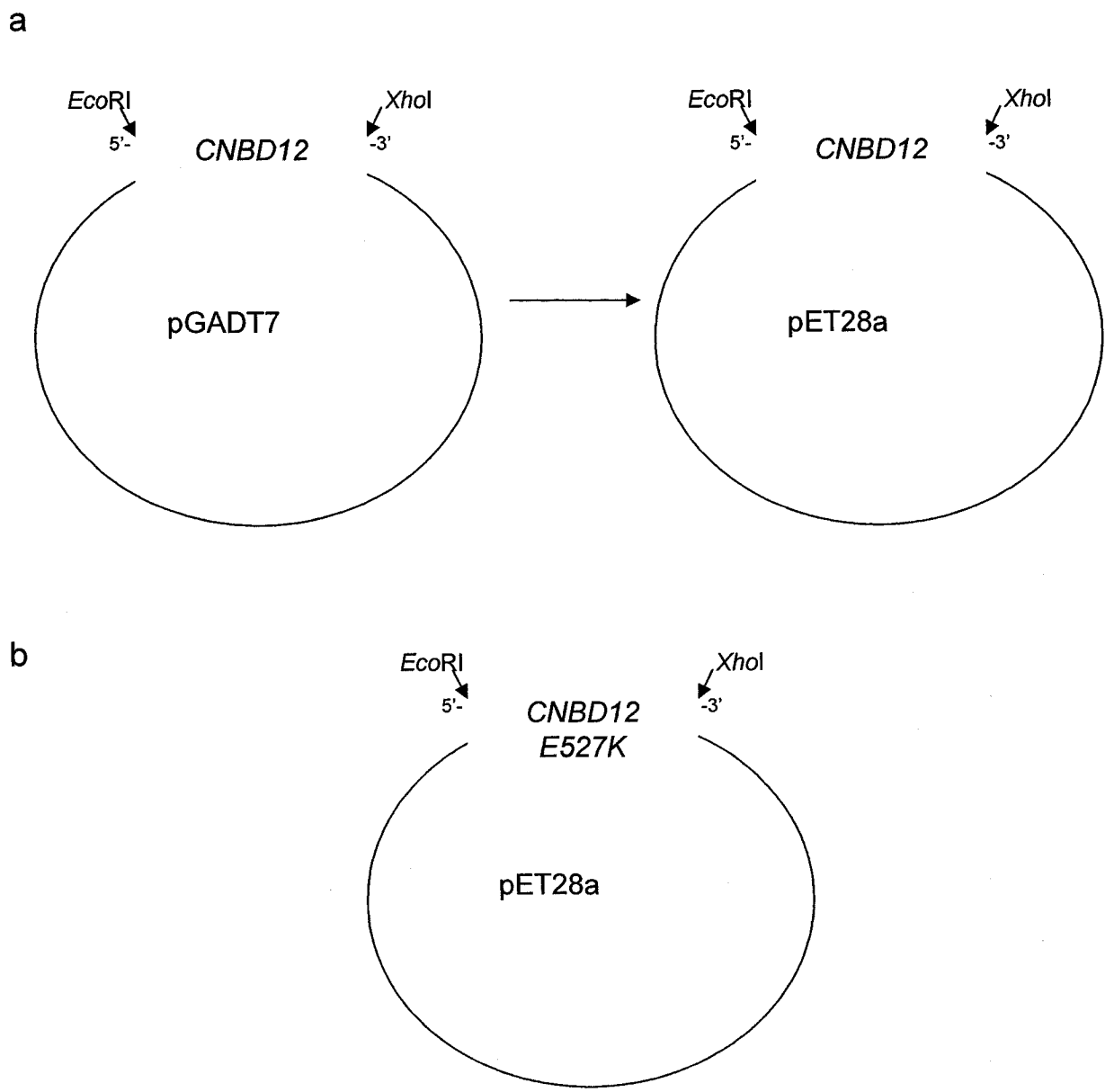

Figure 3. Construction of *CNBD12* and *CNBD12:E527K* in pET28. (a) *CNBD12* cDNA was digested from pGADT7-*CNBD12* by *Eco*RI and *Xho*I and ligated into a pET28a vector digested with the same enzymes. (b) pET28a-*CNBD12:E527K* was created by digesting the DNA product from a PCR using pYES2-*ATCNGC11/12:E519K* as template DNA, and a forward primer that introduced a *Eco*RI site before the T1299 nucleotide (the reverse primer did not change the 3'-end sequence, there is a *Xho*I restriction site at the location indicated).

REFERENCES

Aarts, N., Metz, M., Holub, E., Staskawicz, B.J., Daniels, M.J., and Parker, J.E. (1998) Different requirements for EDS1 and NDR1 by disease resistance genes define at least two *R* gene-mediated signaling pathways in *Arabidopsis*. *Proc. Natl Acad. Sci. USA* **95**: 10306-10311.

Akhavan, A., Atanasiu, R., and Shrier, A. (2003) Identification of COOH-terminal segment involved in maturation and stability of human ether-a-go-go-related gene potassium channels. *J. Biol. Chem.* **278**: 40105-40112.

Akhavan, A., Atanasiu, R., Noguchi, T., Han, W., Holder, N., and Shrier, A. (2005) Identification of the cyclic-nucleotide-binding domain as a conserved determinant of ion-channel cell-surface localization. *J. Cell Sci.* **118**: 2803-2812

Ali, R., Zielinski, R.E., and Berkowitz, G.A. (2006) Expression of plant cyclic nucleotide-gated cation channels in yeast. *J. Exp. Bot.* **57**:125-138.

Anderson, J.A., Huprikar, S.S., Kochian, L.V., Lucas, W.J., and Gaber, R.F. (1992) Functional expression of a probable *Arabidopsis thaliana* potassium channel in *Saccharomyces cerevisiae*. *Proc. Natl. Acad. Sci. USA* **89**:3736-3740.

Arazi, T., Sunkar, R., Kaplan, B., and Fromm, H. (1999) A tobacco plasma membrane calmodulin-binding transporter confers Ni^{2+} tolerance and Pb^{2+} hypersensitivity in transgenic plants. *Plant J.* **20**:171-182.

Balague, C., Lin, B., Alcon, C., Flottes, G., Malmstrom, S., Kohler, C., Neuhaus, G., Pelletier, G., Gaymard, F., and Roby, D. (2003) HLM1, an essential signaling component in the hypersensitive response, is a member of the cyclic nucleotide-gated channel ion channel family. *Plant Cell* **15**:365-379.

Berman, H.M., Ten Eyck, L.F., Goodsell, D.S., Haste, N.M., Kornev, A., and Taylor, S.S. (2005) The cAMP binding domain: An ancient signaling module. *PNAS* **102**: 45-50.

Bihler, H., Slayman, C.L., and Bertl, A. (2002) Low-affinity potassium uptake by *Saccharomyces cerevisiae* is mediated by NSC1, a calcium-blocked non-specific cation channel. *Biochimica et Biophysica Acta* **1558**: 109-118.

Borsics, T., Webb, D., Andeme-Ondzighi, C., Staehelin, L.A., and Christopher, D.A. (2007) The cyclic nucleotide-gated calmodulin-binding channel AtCNGC10 localizes to the plasma membrane and influences numerous growth responses and starch accumulation in *Arabidopsis thaliana*. *Planta* **255**: 563-573.

Bowling, S.A., Clarke, J.D., Liu, Y., Klessig, D.F., and Dong, X. (1997) The *cpr5* mutant of Arabidopsis expresses both NPR1-dependent and NPR1-independent resistance. *Plant Cell* **9**: 1573-1584.

Bowling, S.A., Guo, A., Cao, H., Gordon, A.S., Klessig, D.F., and Dong, X. (1994) A mutation in Arabidopsis that leads to constitutive expression of systemic acquired resistance. *Plant Cell* **6**: 1845-1857.

Bradley, J., Frings, S., Yau, K.W., and Reed, R. (2001) Nomenclature for ion channel subunits. *Science* **294**:2095-2096.

Bradley, J., Reuter, D., and Frings, S. (2001) Facilitation of calmodulin-mediated odor adaptation by cAMP-gated channel subuntis. *Science*294: 2176–2178.

Brunet, L.J., Gold, G.H., and Ngai, J. (1996) General anosmia caused by a targeted disruption of the mouse olfactory cyclic nucleotide-gated cation channel. *Neuron* **17**: 681-693.

Canaves, J.M., and Taylor, S.S. (2002) Classification and phylogenetic analysis of the cAMP-dependent protein kinase regulatory subunit family. *J. Mol. Evol.* **54**: 17-29.

Cao, H., Bowling, S.A., Gordon, A.S., and Dong, X. (1994) Characterization of an Arabidopsis mutant that is nonresponsive to inducers of systemic acquired resistance. *Plant Cell* **6**:1583-1592.

Century, K.S., Holub, E.B., and Staskawicz, B.J. (1995) NDR1, a locus of Arabidopsis thaliana that is required for disease resistance to both a bacterial and fungal pathogen. *Proc. Natl Acad. Sci. USA* **92**: 6597-6601.

Chan, C.W., Schorrak, L.M., Smith, Jr., R.K., Bent, A.F., and Sussman, M.R. (2003) A cyclic nucleotide-gated ion channel, CNGC2, is crucial for plant development and adaptation to calcium stress. *Plant Physiol.* **132**:728-731.

Christopher, D.A., Borsics, T. Yuen, C.Y., Ullmer, W., Andeme-Ondzighi, C., Andres, M.A., Kang, B.H., and Staehelin, L.A. (2007) The cyclic nucleotide gated cation channel AtCNGC10 traffics from the ER via Golgi vesicles to the plasma membrane of *Arabidopsis* root and leaf cells. *BMC Plant Biol.* **7** (In Press)

Clarke, J.D., Liu, Y., Klessig, D.F., and Dong, X. (1998) Uncoupling *PR* gene expression from *NPR1* and bacterial resistance: characterization of the dominant Arabidopsis *cpr6-1* mutant. *Plant Cell* **10**: 557-569.

Clarke, J.D., Volko, S.M., Ledford, H., Ausubel, F.M., and Dong, X. (2000) Roles of salicylic acid, jasmonic acid, and ethylene in cpr-induced resistance in arabidopsis. *Plant Cell* **12**: 2175-2190.

Clough, S.J., Fengler, K.A., Yu, I.C., Lippok, B., Smith, R.K., Jr., and Bent, A.F. (2000) The Arabidopsis dnd1 "defense, no death" gene encodes a mutated cyclic nucleotide-gated ion channel. *Proc. Natl. Acad. Sci. USA* **97**:9323-9328.

Craven, K.B., and Zagotta, W.N. (2004) Salt bridges and gating in the COOH-terminal region of HCN2 and CNGA1 channels. *J. Gen. Physiol.* **124**: 663-677.

Craven, K.B., and Zagotta, W.N. (2006) CNG and HCN channels: two peas, one pod. *Annu. Rev. Physiol.* **68**: 375-401.

Curran, M.E., Splawski, I., Timothy, K.W., Vincent, G.M., Green, E.D., and Keating, M.T. (1995) A molecular basis for cardiac arrhythmia: HERG mutations cause long QT syndrome. *Cell* **80**: 795-803.

DeLano, W.L. (2002) The PyMOL Molecular Graphics System. DeLano Scientific, San Carlos, CA, USA. http://www.pymol.org.

Dangl, J.L., Dietrich, R.A., and Richberg, M.H. (1996) Death don't have no mercy: cell death programs in plant-microbe interactions. *Plant Cell* **8**: 1793-1807.

Delaney, T.P., Friedrich, L., and Ryals, J.A. (1995) *Arabidopsis* signal transduction mutant defective in chemically and biologically induced disease resistance. *Proc. Natl Acad. Sci. USA* **92**: 6602-6606.

Dempsey, D., Shah, J., and Klessig, D.F. (1999) Salicylic acid and disease resistance in plants. *Crit. Rev. Plant Sci.* **18**:547-575.

Dryja, T.P., Finn, J.T., Peng, Y-W., McGee, T.L., Berson, E.L., and Yau, K-W. (1995) Mutations in the gene encoding the α-subunit of the rod cGMP-gated channel in autosomal recessive retinitis pigmentosa. *ProcNatl Acad Sci USA* **92**: 10177–10181.

Feys, B.J., Moisan, L.J., Newman, M.-A., and Parker, J.E. (2001) Direct interaction between the Arabidopsis disease resistance signaling proteins, EDS1 and PAD4. *EMBO J.* **20**: 5400-5411.

Fesenko, E.E., Kolesnikov, S.S, and Lyubarsky, A.L. (1985) Induction by cyclic GMP of cationic conductance in plasma membrane of retinal rod outer segment. *Nature* **313**:310-313.

Ficker, E., Dennis, A.T., Obejero-Paz, C.A., Castaldo, P., Taglialatela, M., and Brown, A.M. (2000) Retention in the Endoplasmic Reticulum as a mechanism of dominant-negative current suppression in human long QT syndrome. *J. Mol. Cell Cardiol.* **32**: 2327-2337.

Ficker, E., Obejero-Paz, C.A., Zhao, S., and Brown, A.M. (2002) The binding site for channel blockers that rescue misprocessed human long QT syndrome type 2 ether-a-gogo-related gene (HERG) mutations. *J. Biol. Chem.* **277**: 4989-4998.

Frietsch, S., Wang, Y.F., Sladek, C., Poulsen, L.R., Romanowsky, S.M., Schroeder, J.I., Harper, and J.F. (2007) A cyclic nucleotide-gated channel is essential for polarized tip growth of pollen. *Proc. Natl. Acad. Sci. USA* **104**: 14531-14536.

Fujikawa, Y., and Kato, N. (2007) Split luciferase complementation assay for studying protein-protein interactions in Arabidopsis protoplasts. *The Plant Journal*: in press.

Gaber, R.F., Styles, C.A. and Fink, G.R. (1988) TRK1 encodes a plasma membrane protein required for high-affinity potassium transport in *Saccharomyces cerevisiae*. *Mol. Cell Biol.* **8**:2848-2859.

Glazebrook, J., Rogers, E.E., and Ausubel, F.M. (1996) Isolation of *Arabisopsis* mutants with enhanced disease susceptibility by direct screening. *Genetics* **143**: 973-982.

Gobert, A., Park, G., Amtmann, A., Sanders, D., and Maathuis, F.J.M. (2006) *Arabidopsis thaliana* Cyclic Nucleotide Gated Channel 3 forms a non-selective ion transporter involved in germination and cation transport. *J. Exp. Botany* **57**:791-800.

Gordon, S.E., and Zagotta, W.N. (1995) Subunit interactions in coordination of Ni2+ in cyclic nucleotide-gated channels. *Pro. Natl. Acad. Sci. USA* **92**: 10222-10226.

Goulding, E.H., Tibbs, G.R. and Siegelbaum, S.A. (1994) Molecular mechanism of cyclic-nucleotide-gated channel activation. *Nature*. **372**: 369-374.

Hammond-Kosack, K.E., and Jones, J.D.G. (1996) Resistance gene-dependent plant defense responses. *Plant Cell* **8**:1773-1791.

Hua, B.G., Mercier, R.W., Leng, Q., and Berkowitz, G.A. (2003) Plants do it differently. A new basis for potassium/sodium selectivity in the pore of an ion channel. *Plant Phys.* **132**: 1353-1361.

Hua, B.G., Mercier, R.W., Zielinski, R.E., Berkowitz, G.A. (2003) Functional interaction of calmodulin with a plant cyclic nucleotide gated cation channel. *Plant Phys. Biochem.* **41**: 945-954.

Johnson, J.P. Jr., and Zagotta, W.N. (2001) Rotational movement during cyclic nucleotide-gated channel opening. *Nature* **412**: 917-921.

Jurkowski, G.I., Smith, R.K., Jr., Yu, I.C., Ham, J.H., Sharma, S.B., Klessig, D.F., Fengler, K.A., and Bent, A.F. (2004). Arabidopsis DND2, a second cyclic nucleotide-gated ion channel gene for which mutation causes the "defense, no death" phenotype. *Mol. Plant Microbe Interact.* **17**: 511–520.

Kachroo, P., Leong, S.A., and Chattoo, B.B. (1995) Mg-SINE: A short interspersed nuclear element from the rice blast fungus, *Magnaporthe grisea. Proc. Natl. Acad. Sci. USA* **92**: 11125–11129.

Kaplan, B., Sherman, T., and Fromm, H. (2007) Cyclic nucleotide-gated channels in plants. *FEBS Letters* **581**:2237-2246.

Kaupp, U.B., Niidome, T., Tanabe, T., Terada, S., Bönigk, W., Stűhmer, Neil., Cook, J., Kangawa, K., Matsuo, H., Hirose, T., Miyata, T., and Numa, S. (1989) Primary structure and functional expression from complementary DNA of the rod photoreceptor cyclic GMP-gated channel. *Nature* **342**: 762-766.

Kaupp, U.B. and Seifert, R. (2002) Cyclic nucleotide-gated ion channels. *Physiol. Rev.* **82**: 769-824.

Kawasaki, H., Springett, G.M., Mochizuki, N., Toki, S., Nakaya, M., Matsuda, M., Housman, D.E., and Graybiel, A.M. (1998) A family of cAMP-binding proteins that directly activate Rap1. *Science* **282**:2275-2279.

Ko, C.H., and Gaber, R.F. (1991) TRK1 and TRK2 encode structurally related K^+ transporters in *Saccharomyces cerevisiae. Mol. Cell Biol.* **11**: 4266-4273.

Kohl, S., Baumann, B., Broghammer, M., Jägle, H., Sieving, P., Kellner, U., Spegal, R., Anastasi, M., Zrenner, E., Sharpe, L.T., and Wissinger, B. (2000) Mutations in the CNGB3 gene encoding the β-subunit of the cone photoreceptor cGMP gated channel are responsible for achromatopsia (*ACHM3*) linked to chromosome 8q21. *Hum. Mol. Genet.* **9**: 2107-2116.

Kohl, S., Marx, T., Giddings, I., Jägle, H., Jacobson, S.G., Apfelstedt-Syllae, E., Zrenner, E., Sharpe, L.T., and Wissinger, B. (1998) Total colour blindness is caused by mutations in the gene encoding the α-subunit of the cone photoreceptor cGMP-gated cation channel. *Nature Genet* **19**: 257–259.

Köhler, C., Merkle, T., and Neuhaus, G. (1999) Characterization of a novel gene family of putative cyclic nucleotide- and calmodulin-regulated ion channels in *Arabidopsis thaliana. Plant J.* **18**:97-104.

Köhler, C., Merkle, T., Roby, D., and Neuhaus, G. (2001) Developmentally regulated expression of a cyclic nucleotide-gated ion channel from Arabidopsis indicates its involvement in programmed cell death. *Planta* **213**:327-332.

Köhler, C., and Neuhaus, G. (1998) Cloning and partial characterization of two putative cyclic nucleotide-regulated ion channels from *Arabidopsis thaliana*, designated CNGC1(Y16327), CNGC2 (Y16328) (PGR98-062). *Plant Physiol.* **116**:1604.

Körschen, H.G., Illing, M., Seifert, R., Sesti, F., Williams, A., Gotzes, S., Colville, C., Müller, F., Dosé, A., Godde, M., Molday, L., Kaupp, U.B., and Molday, R.S. (1995) A 240 kDa protein represents the complete _ subunit of the cyclic nucleotide-gated channel from rod photoreceptor. *Neuron* **15**: 627–636.

Li, X., Boriscs, T., Harrington, H.M., and Christopher, D.A. (2005) Arabidopsis AtCNGC10 rescues potassium channel mutants of *E. coli*, yeast and Arabidopsis and is regulated by calcium/calmodulin and cGMP in *E. coli*. *Func. Plant Biol.* **32**:643-653.

Liu, D.T., Tibbs, G.R., and Siegelbaum, S.A. (1996) Subunit stoichiometry of cyclic nucleotide-gated channels and effects of subunit order on channel function. *Neuron* **16**: 983-990.

Leng, Q., Mercier, R.W., Yao, W., and Berkowitz, G.A. (1999) Cloning and first functional characterization of a plant cyclic nucleotide-gated cation channel. *Plant Physiol.* **121**: 753-761

Leng, Q., Mercier, R.W., Hua, B.G., Fromm, H., and Berkowitz, G.A. (2002) Electrophysiological analysis of cloned cyclic nucleotide-gated ion channels. *Plant Physiol.* **128**: 400-410.

Lu, H., Rate, D.N., Song, J.T., and Greenberg, J.T. (2003) ACD6, a novel ankyrin protein, is a regulator and an effector of salicylic acid signaling in the Arabidopsis defense response. *Plant Cell* **15**: 2408-2420.

Lu, H., Liu, Y., and Greenberg, J.T. (2005) Structure-function analysis of the plasma membrane-localized Arabidopsis defense component ACD6. *Plant J.* **44**: 798-809.

Ma, W., Ali, R., and Berkowitz, G.A. (2006) Characterization of plant phenotypes associated with loss-of-function of AtCNGC1, a plant cyclic nucleotide gated cation channel. *Plant Physiol. Biochem.* **44**:494-505.

Madrid, R., Gomez, M.J., Ramos, J., and Rodriquez-Navarro, A. (1998) Ectopic potassium uptake in trk1 trk2 mutants of *Saccharomyces cerevisiae* correlates with a highly hyperpolarized membrane potential. *J. Biol. Chem.* **273**: 14838-14844.

Mallory, A.C., Parks, G., Endres, M.W., Baulcombe, D., Bowman, L.H., Pruss, G.J., and Vance, V.B. (2002) The amplicon-plus system for high-level expression of transgenes in plants. *Nature* **20**: 622-625.

Mäser, P., Thomine, S., Schroeder, J.I., Ward, J.M., Hirschi, K., Sze, H., Talke, I.N., Amtmann, A., Maathuis, F.J., Sanders, D., Harper, J.F., Tchieu, J., Gribskov, M., Persans, M.W., Salt, D.E., Kim, S.A., and Guerinot, M.L. (2001) Phylogenetic relationships within cation transporter families of *Arabidopsis*. *Plant Physiol.* **126**:1646-1667.

Matulef, K., Flynn, G.E., and Zagotta, W.N. (1999) Molecular rearrangements in the ligand-binding domain of cyclic nucleotide-gated channels. *Neuron* **24**:443-452.

Matulef, K., and Zagotta, W.N. (2003) Cyclic Nucleotide-Gated Ion Channels. *Annu. Rev. Cell Dev. Biol.* **19**:23-44.

McDonnell, A.V., Jiang, T., Keating, A.E. and Berger, B. (2006) Paircoil2: improved prediction of coiled coils from sequence. *Bioinformatics* **22**: 356-358.

Mercier, R.W., Rabinowitz, N.M., Ali, R., Gaxiola, R.A., and Berkowitz, G.A. (2004). Yeast hygromycin sensitivity as a functional assay of cyclic nucleotide gated cation channels. *Plant Physiol. Biochem.* **42**: 529–536.

Moeder, W., Del Pozo, O., Navarre, D.A., Martin, G.B, and Klessig, D.F. (2007) Aconitase plays a role in regulating resistance to oxidative stress and cell death in Arabidopsis and *Nicotiana benthamiana. Plant Mol. Biol.* **63**: 273-287.

Munger, S.D., Lane, A.P., Zhong, H., Leinders-Zufall, T., Yau, K-W., Zufall, F., and Reed, R.R. (2001) Central role of the CNGA4 channel subunit in Ca^{2+}-calmodulin-dependent odor adaptation. *Science* **294**: 2172-2175.

Nakamura, T., and Gold, G.H. (1987) A cyclic nucleotide-gated conductance in olfactory receptor cilia. *Nature* **325**:442-444.

Proenza, C., Tran, N., Angoli, D., Zahynacz, K., Balcar, P., and Accili, E.A. (2002) Different roles for the cyclic nucleotide binding domain and amino terminus in assembly and expression of hyperpolarization-activated, cyclic nucleotide-gated channels. *J. Biol. Chem.* **277**: 29634-29642.

Punta, M., Cavalli, A., Torre, V., and Carloni, P. (2003) Molecular modeling studies on CNG channel from bovine retinal rod: a structural model of the cyclic nucleotide-binding domain. *Proteins: struc., func., genet.* **52**: 332-338.

Rate, D.N., Cuence, J.V., Bowman, G.R., Guttman, D.S., and Greenberg, J.T. (1999) The gain-of-function Arabidopsis *acd6* mutant reveals novel regulation and function of the salicyclic acid signaling pathway in controlling cell death, defenses, and cell growth. *Plant Cell* **11**: 1695-1708.

Rehmann, H., Wittinghofer, A., and Bos, J.L. (2007) Capturing cyclic nucleotides in action: snapshots from crystallographic studies. *Nat. Rev. Mol. Cell Biol.* **8**: 63-73.

Robinson, R.B., and Siegelbaum, S.A. (2003) Hyperpolarization-activated cation currents: from molecules to physiological function. *Annu. Rev. Physiol.* **65**: 453-480.

Rostoks, N., Schmierer, D., Mudie, S., Drader, T., Brueggeman, R., Caldwell, D.G., Waugh, R., and Kleinhofs, A. (2006) Barley necrotic locus nec1 encodes the cyclic

nucleotide-gated ion channel 4 homologous to the Arabidopsis HLM1. *Mol. Genet. Genomics* **275**: 159-168.

Sambrook, J., and Russell, D.W. (2001) Molecular Cloning: A laboratory manual. Cold Spring Harbor Laboratory Press, Cold Spring Harbor, New York, USA.

Sanguinetti, M.C., Jiang, C., Curran, M.E., and Keating, M.T. (1995) A mechanistic link between an inherited and an acquired cardiac arrhythmia: HERG encodes the Ikr potassium channel. *Cell* **80**: 299-307.

Satler, C.A., Walsh, E.P., Vesely, M.R., Plummer, M.H., Ginsburg, G.S., and Jacob, H.J. (1996) Novel missense mutation in the cyclic nucleotide-binding domain of HERG causes long QT syndrome. *Am. J. Med. Genet.* **65**: 27-35.

Schuurink, R.C., Shartzer, S.F., Fath, A., and Jones, R.L. (1998) Characterization of a calmodulin-binding transporter from the plasma membrane of barley aleurone. *Proc. Natl. Acad. Sci. USA* **95**:1944-1949.

Scott, S-P., and Tanaka, J.C. (1995) Molecular interactions of 3', 5'-cyclic purine analogues with the binding site of retinal rod ion channels. *Biochemistry* **34**: 2338-2347.

Scott, S-P., Cummings, J., Joe, J.C., and Tanaka, J.C. (2000) Mutating three residues in the bovine rod cyclic nucleotide-activated channel can switch a nucleotide from inactive to active. *Biophys J.* **78**: 2321-2333.

Scott, S-P., Shea, P.W., and Dryer, S.E. (2007) Mapping ligand interactions with the hyperpolarization activated cyclic nucleotide modulated (HCN) ion channel binding domain using a soluble construct. *Biochemistry* (In Press).

Sessa, G., D'Ascenzo, M., and Martin, G.B. (2000) Thr38 and Ser198 are Pto autophosphorylation sites required for the AvrPto-Pto-mediated hypersensitive response. *EMBO J.* **19**: 2257-2269.

Sentenac, H., Bonneaud, N., Minet, M., Lacroute, F., Salmon, J-M., Gaymard, F., and Grignon, C. (1992) Cloning and expression in yeast of a plant potassium ion transport system. *Science* **256**: 663-665.

Shah, J., Tsui, F., and Klessig, D.F. (1997) Characterization of a salicylic acid-insensitive mutant (*sai1*) of *Arabidopsis thaliana*, identified in a selective screen utilizing the SA-inducible expression of the *tms2* gene. *Mol. Plant-Microbe Interact.* **10**: 69-78.

Shapiro, M.S., and Zagotta, W.N. (2000) Structural basis for ligand selectivity of heteromeric olfactory cyclic nucleotide-gated channels. *Biophys. J.* **78**: 2307-2320.

Sundin, O.H., Yang, J-M., Li, Y., Zhud, D., Hurd, J.N., Mitchell, T.N., Silva, E.D., and Maumenee, I.H. (2000) Genetic basis of total colour blindness among

the Pingelapese islanders. *Nature Genet* **25**: 289–293.

Sunkar, R., Kaplan, B., Bouche, N., Arazi, T., Dolev, D., Talke, I.N., Maathuis, F.J., Sanders, D., Bouchez, D., and Fromm, H. (2000) Expression of a truncated tobacco NtCBP4 channel in transgenic plants and disruption of the homologous *Arabidopsis* CNGC1 gene confer Pb^{2+} tolerance. *Plant J.* **24**:533-542.

Talke, I.N., Blaudez, D., Maathuis, F.J., and Sanders, D. (2003) CNGCs: prime targets of plant cyclic nucleotide signaling? *Trends Plant Sci.* **8**: 286-293.

Tanaka, J.C., Eccleston, J.F., and Furman, R.E. (1989) Photoreceptor channel activation by nucleotide derivatives. *Biochemistry* **28**: 2776-2784.

Taraska, J.W., and Zagotta, W.N. (2007) Structural dynamics in the gating ring of cyclic nucleotide-gated ion channels. *Nature Struc. Mol. Biol.* **14**: 854-860.

Thompson, J.D., Higgins, D.G. and Gibson, T.J. (1994), CLUSTAL W: improving the sensitivity of progressive multiple sequence alignment through sequence weighting, position specific gap penalties and weight matrix choice. *Nucleic Acids Research.*

Uemura, T., Ueda, T., Ohniwa, R.L., Nakano, A., Takeyasu, K., and Sato, M.H. (2004) Systematic analysis of SNARE molecules in Arabidopsis: dissection of the post-Golgi network in plant cells. *Cell Struct Funct* **29:** 49-65.

Urquhart, W., Gunawardena, A.H.L.A.N., Moeder, W., Ali, R., Berkowitz, G.A. and Yoshioka, K. (2007) The chimeric cyclic nucleotide-gated ion channel ATCNGC11/12 constitutively induces programmed cell death in a Ca^{2+} dependent manner. *Plant Mol. Biol.* (In Press)

Varnum, M.D., Black, K.D., and Zagotta, W.N. (1995) Molecular mechanism for ligand discrimination of cyclic nucleotide-gated channels. *Neuron* **15**: 619-625.

Varnum, M.D., and Zagotta, W.N. (1996) Subunit interactions in the activation of cyclic nucleotide-gated ion channels. *Biophys. J.* **70**: 2667-2679.

Weber, I.T., and Steitz, T.A. (1987) Structure of a complex of catabolite gene activator protein and cyclic AMP refined at 2.5 Å resolution. *J. Mol. Biol.* **198**: 311-326.

Wei, J.Y., Cohen, E.D., Yan,Y.Y., Geniesser, H.G., and Barnstable, C.J. (1996) Identification of competitive antagonists of the rod photoreceptor cGMP-gated cation channel: beta-phenyl-1,N2-etheno-substituted cGMP analogues as probes of the cGMP-binding site. *Biochemistry* **35**: 16815-16823.

Weigel, D., and Glasebrook, J. (2002) Arabidopsis: A laboratory manual. Cold Spring Harbor Laboratory Press, Cold Spring Harbor, New York, USA.

Weitz, D., Ficek, N., Kremmer, E., Bauer, P.J., and Kaupp, U.B. (2002) Subunit stoichiometry of the CNG channel of rod photoreceptors. *Neuron* **36**: 881-889.

Wildermuth, M.S., Dewdney, J., Wu., G., and Ausubel, F.M. (2002) Isochorismate synthase is required to synthesize salicylic acid for plant defense. *Nature* **414**: 562-566.

Wissinger, B., Gamer, D., Jagle, H., Giordar, R., Marx, T., Mayer, S., Tippmann, S., Broghammer, M., Jurklies, B., Rosenberg, T., Jacobson, S.G., Sener, E.C., Tatlipinar, S., Hoyng, C.B., Castellan, C., Bitoun, P., Andreasson, S., Rudolph, G., Kellner, U., Lorenz, B., Wolff, G., Verellen-Dumoulin, C., Schwartz, M., Cremers, F.P., Apfelstedt-Sylla, E., Zrenner, E., Salati, R., Sharpe, L.T., and Kohl, S. (2001) CNGA3 mutations in hereditary cone photoreceptor disorders. *Am J Hum Genet* **69**: 722–737.

Yau, K-W., and Baylor, D.A. (1989) Cyclic GMP-activated conductance of retinal photoreceptor cells. *Annu. Rev. Neurosci.* **12**: 289-327.

Yoshioka, K., Kachroo, P., Tsui, F., Sharma, S.B., Shah, J., and Klessig, D.F. (2001). Environmentally-sensitive, SA-dependent defense response in the *cpr22* mutant of Arabidopsis. *Plant J.* **26**: 447–459.

Yoshioka, K., Moeder, W., Kang, H-G., Kachroo, P., Masmoudi, K., Berkowitz, G., and Klessig, D.F. (2006) The chimeric *Arabidopsis* cyclic nucleotide-gated ion channel 11/12 activates multiple pathogen resistance responses. *Plant Cell.* **18**: 747-763.

Yoo, S.-D., Cho, Y.-H., and Sheen, J. (2007) *Arabidopsis* Mesophyll Protoplasts: A Versitile Cell System for Transient Gene Expression Analysis. *Nature Protocols* **2**:1565-1572.

Yu, I.C., Parker, J., and Bent, A.F. (1998) Gene-for-gene disease resistance without the hypersensitive response in *Arabidopsis dnd1* mutant. *Proc. Natl. Acad. Sci. USA* **95**: 7819-7824.

Zagotta, W.N., and Siegelbaum, S.A. (1996) Structure and function of cyclic nucleotide-gated channels. *Annu. Rev. Neurosci.* **19**: 235-263.

Zagotta, W.N., Olivier, N.B., Black, K.D., Young, E.C., Olson, R., and Gouaux, E. (2003) Structural basis for modulation and agonist specificity of HCN pacemaker channels. *Nature* **425**: 200-205.

Zheng, J., Trudeau, M.C., and Zagottat, W.N. (2002) Rod cyclic nucleotide-gated channels have a stoichiometry of three CNGA1 subunits and one CNGB1 subunit. *Neuron* **36**: 891-896.

Zhong, H., Molday, L.L., Molday, R.S., and Yau, K-W. (2002) The heteromeric cyclic nucleotide-gated channel adopts a 3A:1B stoichiometry. *Nature* **420**: 193-198.

Zhou, Z., Gong, Q., Epstein, M. L., and January, C. T. (1998) HERG channel dysfunction in human long QT syndrome. *J. Biol. Chem.* **273**: 21061–21066.